General Disclaimer

One or more of the Following Statements may affect this Document

- This document has been reproduced from the best copy furnished by the organizational source. It is being released in the interest of making available as much information as possible.

- This document may contain data, which exceeds the sheet parameters. It was furnished in this condition by the organizational source and is the best copy available.

- This document may contain tone-on-tone or color graphs, charts and/or pictures, which have been reproduced in black and white.

- This document is paginated as submitted by the original source.

- Portions of this document are not fully legible due to the historical nature of some of the material. However, it is the best reproduction available from the original submission.

Produced by the NASA Center for Aerospace Information (CASI)

ANALYTICAL AND NUMERICAL INVESTIGATION OF STRUCTURAL RESPONSE OF COMPLIANT WALL MATERIALS

By

R. Balasubramanian

G.L. Goglia, Principal Investigator

Final Report

March 1978

DEPARTMENT OF MECHANICAL ENGINEERING AND MECHANICS
SCHOOL OF ENGINEERING
OLD DOMINION UNIVERSITY
NORFOLK, VIRGINIA

ANALYTICAL AND NUMERICAL INVESTIGATION OF STRUCTURAL

RESPONSE OF COMPLIANT WALL MATERIALS

By

R. Balasubramanian

G.L. Goglia, Principal Investigator

Final Report

March 1978

TABLE OF CONTENTS

LIST OF TABLES

LIST OF FIGURES

ANALYTICAL AND NUMERICAL INVESTIGATION OF STRUCTURAL
RESPONSE OF COMPLIANT WALL MATERIALS

By

R. Balasubramanian[1]

SUMMARY

Theoretical analysis of an electrostatically driven wall system for a
compliant wall drag reduction program is reported. The electrostatic wall
system is capable of producing deflections of many orders greater than the
thicknesses and at small wavelengths. An intermediate large response theory
is used for structural analysis. The theoretical predictions are compared to
bench test results, and good agreement between the two is obtained. The effects
of aerodynamic loads and perturbation electric fields on the theoretical
solutions are considered. It is shown that for very small wavelengths
($\lambda \approx 2$ mm) the aerodynamic effects can be estimated using potential theory
without loss of accuracy, and the perturbation electric fields do not affect
solutions as long as the deflections are less than one percent of the wave-
length. Resonance effects for this type of structure are shown to be fairly
small.

1. INTRODUCTION

Details of the compliant wall drag reduction program at Langley have
been discussed in a supplementary report (ref. 1) under the present contract
NSG 1236. It was pointed out in that report that passive walls with short
wavelengths and large amplitudes are extremely difficult to design. Extension
of grant NSG 1236 was given in order to design controlled active wall experi-
ments. The amplitude of surface motion desired was given to be in the range
of 5×10^{-5} m to 2×10^{-4} m, the wavelength of the surface motion in the range
2.5×10^{-3} m to 6×10^{-3} m, and the frequency range to be between 300 Hz and

---

[1] Research Associate, Old Dominion University Research Foundation,
Norfolk, Virginia 23508.

2 kHz. After careful evaluation of existing techniques for active wall
experiments (refs. 2 to 4) it was decided to develop an active wall system using
electrostatic forces as loading to the structure. The choice of materials
for this system was narrowed to extremely thin elastomers, and the amplitude
constraint given above dictated large values of the ratio of amplitude thick-
ness. A nonlinear structural response analysis was conducted to determine
accurate surface motion predictions. In sections 2 to 4 the electrostatic
wall system is discussed in detail, and in section 5 comparisons with experi-
mental measurements are reported.

2. ANALYSIS OF THE ELECTROSTATIC WALL PROBLEM

The recent summary paper (ref. 5) suggests that low-speed air experiments
for compliant wall drag reduction be conducted with controlled or active wall sur-
face motion to assess the nature of possible turbulent boundary layer modifications
due to the wall motion. Previous active wall experiments reported in the litera-
ture (refs. 2 to 4) used mechanical drivers; these drive systems are inadequate for
producing high-frequency, short-wavelength motion contemplated for active wall experi-
ments at Langley. The present work describes an electrostatic wall designed to
operate in a frequency range of 200 Hz to 10 kHz with two-dimensional standing waves
of wavelength 2×10^{-3} to 10^{-2} m. The structural surface is basically a thin elec-
trically conducting elastomer membrane with a series of transverse electrodes etched
on a PC board as exciters. The structure is periodic, supported at discrete lines
by transverse ribs. Figure 1 shows the electrostatic wall system along with the
electrical hookup. Referring to figure 1, the output from the transformer T
is biased at the center-tap and connected to the terminals A and B as indicated.
The conducting membrane surface of width b and thickness h and isotropic
properties (Young's modulus E, density ρ, Poisson's ratio ν) is supported
structurally at separations of length ℓ, where $\ell << b$; the membrane surface
is electrically grounded. The electrodes are equally spaced from one another
and at a separation H from the membrane surface, and they are connected
alternately to terminals A or B. Each periodic bay of the conducting surface
has a sealed cavity of volume $V(H \times \ell \times b)$ underneath it.

The electrostatic wall model is designed to operate at a frequency range of
200 Hz to 10 kHz. The largest dimension of the model is about 0.4 m, speci-
fically for testing at the 7 in. × 11 in. tunnel facility at Langley. The
largest nondimensional speed is

$$\frac{\omega L}{c_o} = \frac{0.4 \times 2\pi \times 10000}{3 \times 10^8} \ll 1 \tag{2.1}$$

where $\omega = 2\pi f_{max}$ and c_o is the speed of light. Hence, the electric field between the electrodes and the membrane is quasi-static.

When the electrodes carry voltages, an electric field is set up between the membrane and electrodes and the membrane is subjected to a force field. The membrane deflects under this loading thereby altering electric field distribution. For the case where the electric field is only a weak function of the surface undulation, it is possible to uncouple the electric field into a primary field (field with no structural motion) and a perturbation secondary field which is dependent on the amplitude of the structural motion. The deflection of the surface can also be split into a primary deflection (under the loading due to the primary field) and a perturbation field, i.e.,

$$\tilde{E} = \tilde{E}_0 + \tilde{E}_1(w, \tilde{E}_0)$$

$$w = w(\tilde{E}_0) + w_1(w(\tilde{E}_0), \tilde{E}) \tag{2.2}$$

where $\tilde{E}_1 \ll \tilde{E}_0$ and hence $w_1 \ll \omega(\tilde{E}_0)$

3. STRUCTURAL ANALYSIS OF THE MEMBRANE ON PERIODIC SUPPORTS

3.1. Basic Approximations to Structural Analysis

We shall make the following assumptions with regard to the structure under consideration:

(i) The structure is a thin elastic membrane with isotropic properties (Young's modulus E, density ρ and Poisson's ratio $= \nu$).

(ii) The structure is rectangular, flat, and simply supported periodically at distances ℓ. Each periodic bay is identical with regard to the loading on it, etc.

(iii) Beneath each bay of the structure is a cavity which is filled with an incompressible fluid. Hence any transverse motion of the structure should be so as not to decrease the overall volume of this cavity.

3.2. Justification of the Basic Approximations

We shall now examine the above assumptions for the case of a typical electrostatic wall as designed:

(a) The elastomer used was a membrane of thickness between 2.5 μm to 25 μm. (Four thicknesses were actually used: 25 μm, 12.5 μm, 6.25 μm, and 2.5 μm). The membrane was uniform and was an elastic material with $\nu = 0,3$, $\rho = 148$ N/m^3, and $E = 4 \times 10^8$ N/m^2. In order to make the membrane conducting, it was aluminized on one side. The process of aluminizing did not change its uniformity nor its elastic properties in any considerable way, hence the validity of the assumption (i).

(b) The membrane was usually stretched smooth and placed flat over supports which were nylon threads. The supports were spaced equally from one another. The nylon threads were cylindrical in shape and were glued to the membrane with a uniform coating of epoxy resin of negligible thickness. In all cases of construction the flatness of the surface was checked using an optical setup and was found to be extremely good. The excitation field on the membrane was obtained using a symmetrically arranged array of electrodes which were etched on a PC board. The electrodes had a flat geometry, were of identical thickness and breadth, and were equally spaced. The alternate electrodes were connected to terminals A and B of a voltage source. Negligible current was drawn by the resistance of the wires, and hence a constant potential difference existed between terminals A and B. The electrostatic loading on the membrane was therefore identical between bays for the form of applied voltages V_A and V_B (see section 4 for the analysis of the electrostatic loading). Other forms of loading that might occur on the bays include fluid loadings due to static pressure differential appearing across the membrane (the static pressure difference can be held constant or nulled using control valves for adjusting the back pressure of the cavities) and dynamic loadings induced by turbulence (if tested in a wind tunnel with flow over the membrane) and loadings due to fluid structure interaction. The main body of the present analysis and experimental verification was for bench models where the fluid loadings were zero, and hence the fluid loading effects are not considered here. However, in a later section we include these cases and indicate how such cases can be included in analysis for an accurate prediction of the ensuing structural motion.

(c) The cavity underneath the membrane was of uniform depth of about 6 μm or 10 μm. For a membrane with a width of about 0.2 m and periodic length of 0.01 m or less, the volume of the cavity is 2×10^{-8} m^3 for the worst case. For a volume change of 0.01 percent of the total volume by any form of motion of the structure, the bay would have to suffer a loading of 1 kg/m^2. Since the electrostatic forces acting on the membrane in each bay are orders of magnitudes lower in strength, such a change in volume is not possible during the motion of the membrane. In other words, the spring stiffness of the cavity for motions which tend to change the volume is many orders of magnitude greater than the stiffness (of the structure + cavity) for motions where no such compression occurs (i.e. the stiffness of the structure in a deep cavity or in vacuo). For the example considered above, the stiffness introduced by the cavity for motions where change in volume occurs is

$$k_1 = \Delta F / \Delta V = 10^9 \text{ kg/m}^3,$$

which is very large compared to the in vacuo stiffness of the struture. Based on the above discussion it becomes apparent that assumptions (i), (ii), and (iii) in section 2.1 are justifiable approximations to a structural analysis.

3.3. Structural Response Theory for Transverse Motions
of the Periodic Membrane

The undamped structural response in transverse motion of a simply supported rectangular periodic membrane is given by

$$\rho h \frac{\partial^2 w}{\partial t^2} + \left[\frac{Eh^3}{12(1-\nu^2)} \right] \left(\frac{\partial^2}{\partial x^2} + \frac{\partial^2}{\partial y^2} \right)^2 w - \left[N_x \frac{\partial^2 w}{\partial x^2} + N_y \frac{\partial^2 w}{\partial y^2} + N_{xy} \frac{\partial^2 w}{\partial x \partial y} \right] = p^e \quad (3.1)$$

where the quantity $\dfrac{Eh^3}{12(1 - \nu^2)}$ is the flexural rigidity of the membrane, p^e is the total loading (in vacuo external load and the fluid loading), N_x, N_y, N_{xy} are the midplane forces, and w is the transverse motion of the membrane.

To evaluate the midplane forces, one must have an idea of the nature of the loading on the structure. Based on a classification of the external loading we

can classify three distinct regions of structural response. To fix the above motion, let us use the following nondimensionalization.

$$\frac{w}{\ell} = a, \quad \frac{h}{\ell} = q; \quad \frac{t}{\ell}\sqrt{\frac{E}{\rho}} = \tau; \quad \frac{N}{Eh} = \bar{N};$$

$$\frac{P\ell}{Eh} = \bar{p}; \quad \frac{x}{\ell} = \bar{x}; \quad \frac{y}{\ell} = \bar{y} \tag{3.2}$$

Equation (3.1) in nondimensional form is given as,

$$\frac{\partial^2 a}{\partial \tau^2} + \left[\frac{1}{12(1-\nu^2)}\right]\gamma^2\left[\frac{\partial^2}{\partial \bar{x}^2} + \frac{\partial^2}{\partial \bar{y}^2}\right]^2 a - \left[\bar{N}_x\frac{\partial^2}{\partial \bar{x}^2} + \bar{N}_y\frac{\partial^2}{\partial \bar{y}^2} + \bar{N}_{xy}\frac{\partial^2}{\partial \bar{x}\partial \bar{y}}\right]a$$

$$\equiv \bar{p}^e \tag{3.3}$$

For the case where the initial stretching forces applied at the edges of the membrane (i.e. the forces $\bar{N}_{xo}$, $\bar{N}_{yo}$, $\bar{N}_{xyo}$ are all positive, the effect of these tensile forces is to limit the amplitude of motion and thus raise the effective stiffness to transverse motion of the structure. When the initial fields $\bar{N}_{xo}$, $\bar{N}_{yo}$, $\bar{N}_{xyo}$ are negative, the fields are compressive and instability of the structure may occur (i.e. buckling instability).

When the initial compressive stresses are large enough to cause buckling, the rectangular membrane will no longer be flat, but will have a deformed shape under these compressive loads. With the presence of the cavity the initial shape of the membrane is very complicated possibly with local buckling within the bay at some points, etc. This situation is rather unpredictable because of precise knowledge of the initial tension or compression, especially for such flimsy structures. Since it is very difficult to apply compressive stresses while mounting, usually care is taken to keep the membrane with zero initial tension. The subsequent analysis and prediction are simplified by the assumption of zero initial tension.

The following classification of structural response requirements is made with the assumption that the periodic bay is short compared to the width and the initial tension field is zero, i.e., b >> ℓ and $N_{xo} = N_{yo} = N_{xyo} = 0$.

Regime I: small amplitude theory. - The region of applicability of this theory is for $\frac{w}{h} = a/\gamma < 0.10$; thus, this analysis is valid for load parameter $\bar{p}_e < \frac{1.6\pi^4}{12(1 - \nu^2)} \frac{1}{\gamma^3}$. The structural response can be conducted using $N_x = N_y = N_{xy} = 0$ in equation (3.3). The transverse motion is therefore decoupled from inplane motions for this case.

Regime II: (intermediate) large response theory. - For this regime the midplane forces are no longer negligible. For analysis of this case, Von Karman's theory is employed. For the type of flimsy materials we use, even at very large amplitudes the structure is within elastic limits. Based on an order of magnitude analysis of terms such as u_x^2 compared to terms like u_x, w_x^2 we suggest that the intermediate large response theory we develop is valid for $\frac{w}{h} < \frac{0.03}{\gamma}$ or for load parameter $p_e \lesssim 0.008$.

Regime III: large amplitude theory (for $p_e > 0.008$.) - For this region there are very few available methods of solution. The analysis should incorporate large rotation effects. Equation (3.1) is not valid for such analysis. For static cases Reissner's theory has been used with some regularity. The problem is a fully three-dimensional elasticity problem with all components of motion fully coupled with each other. Little progress has been made in this area over the years. Experimental studies in these amplitude ranges are few, and most have been using plates which are fairly thick (compared to the thickness of 6 μm with which we are dealing). Even before the small deformation implied in the theory for Region II becomes invalidated, it happens more often than not that the tensile stresses under large amplitude motion go beyond tensile strength limits. The structure becomes locally plastic, and we no longer can use the isotropy assumptions implied in the analysis.

For flimsy materials such as we use, the maximum tensile stresses induced in large amplitude static motion are given by

$$\sigma_t = \frac{E}{1 - \nu^2} \left(\frac{2\pi}{\ell}\right)^2 \frac{w^2}{8} + \frac{Eh}{12(1 - \nu^2)} \left(\frac{2\pi}{\ell}\right)^2 w$$

$$= \left(\frac{E}{1 - \nu^2}\right)\left(2\pi^2\right)\left[\frac{w^2}{\ell^2} \frac{1}{8} + \frac{h}{\ell} \frac{w}{\ell}\right] \tag{3.4}$$

7

This stress should be below the tensile strength of the material we use, if assumptions of isotropy are to be valid. For the periodic structure we are using in our analysis, the longitudinal intertial effects are negligible as will be shown later in the analysis, and hence the large amplitude vibration problem can be viewed as a quasi-steady problem, especially while evaluating stresses. Hence the bound on the limits of an analysis such as that for Region II will definitely fail if

$$\sigma_t < \sigma_{ts}$$

where σ_{ts} = tensile strength of the structure.

For the polyester film we use as the structural material the tensile strength $\sigma_{ts} = 1.5 \times 10^7$ N/m^2 and $E = 4 \times 10^8$ N/m^2; the smallest wavelength used was $\lambda = 1.814$ mm and the thinnest membrane had a thickness of $h = 2.54$ μm. From equation (3.4) we obtaine the maximum limit on w/h beyond which the structure will be at least locally plastic as

$$\frac{w}{h} \simeq \sqrt{\frac{\sigma_{Ts}*4*(1 - \nu^2)}{E \times \pi^2 * \gamma^2}} = \frac{2}{\pi\gamma}\sqrt{\frac{(1 - \nu^2)\sigma_{Ts}}{E}} = 84.0 \qquad (3.5)$$

We had given the limit for validity of analysis for Region II by consideration of the small deformation approximation implied in it as

$$\frac{w}{h} = \frac{0.03}{\gamma} = \underline{21.5} \ , \qquad (3.6)$$

for $\alpha = 1.4 \times 10^{-3}$, a typical case. Hence, it is feasible using the structure we are designing to study the limits of validity of the moderate large amplitude analysis for the first time in our knowledge.

3.4. Structural Response Theory for (Intermediate)
Large Responses of the Periodic Structure

Equation (3.3) in nondimensional form represents the governing equation for transverse motion of the structure. We make assumptions (i), (ii) and (iii) of section 3.1 in our analysis; i.e. $b \gg \ell$ and

$$\iint_V w \; dx \; dy = 0$$

furthermore, we assume that the excitation field is of the form

$$\int_0^\ell \bar{p}_e \sin \frac{m\pi x}{\ell} \; dx = 0 \quad \text{for } m = \text{odd numbers} \tag{3.7}$$

where $\bar{p}_e$ is the loading function in each bay. The excitation field that will be derived in the next section can be shown to be of the above form for a given form of voltages at terminals A and B of the electrostatic setup.

For a simply supported rectangular bay, the deflection shape can therefore be only of the form

$$w = \sum_m \sum_n w_{mn} \sin \frac{2m\pi x}{\ell} \sin \frac{n\pi y}{b} \tag{3.8}$$

Furthermore, because of uniformity of the electrostatic field in the y direction, the choice of the deflection shape is restricted to

$$w = \sum_m \sum_n w_{mn} \sin \frac{2m\pi x}{\ell} \sin (2n - 1) \frac{\pi y}{b} \tag{3.9}$$

or, in nondimensional form,

$$a = \sum_m \sum_n a_{mn} \sin(2m\pi \bar{x}) \sin(2n - 1)(\pi \bar{y} \beta)$$

where $\beta = \ell/b$ $\tag{3.10}$

defining:

$$\bar{m} = 2m\pi \tag{3.11}$$

(cont'd)

9

$$\beta_{\bar{n}} = (2n - 1)\beta\pi$$

yields

$$a = \sum\sum a_{mn}^{(\tau)} \sin \bar{m}\,\bar{x} \sin \beta_{\bar{n}}\bar{y} \qquad (3.11)$$
$$\text{(concl'd)}$$

3.4.1. Midplane forces. - During deflection under transverse load the midplane suffers in plane strains E_{xx}, E_{yy}, E_{xy}. Assuming that the external load parameter extends through Region II, we define the midplane forces as

$$N_x = \frac{Eh}{(1 - \nu^2)} \left(E_{xx} + \nu E_{yy} \right)$$

$$N_y = \frac{Eh}{(1 - \nu^2)} \left(E_{yy} + \nu E_{xx} \right)$$

$$N_{xy} = \frac{Eh}{2(1 + \nu)} \left(E_{xy} \right) \qquad (3.12)$$

In terms of the nondimensionalization adopted in equation (3.2):

$$\bar{N}_x = \frac{1}{1 - \nu^2} \left[E_{\overline{xx}} + \nu E_{\overline{yy}} \right]$$

$$\bar{N}_y = \frac{1}{1 - \nu^2} \left[E_{\overline{yy}} + \nu E_{\overline{xx}} \right]$$

$$\bar{N}_{xy} = \frac{1}{2(1 + \nu)} E_{\overline{xy}} \qquad (3.13)$$

The midplane strains are related to the components of deformation as

$$E_{\overline{xx}} = \frac{\partial \bar{u}}{\partial \bar{x}} + \frac{1}{2} \left(\frac{\partial a}{\partial \bar{x}} \right)^2$$

$$E_{\overline{yy}} = \frac{\partial \bar{v}}{\partial \bar{y}} + \frac{1}{2} \left(\frac{\partial a}{\partial \bar{y}} \right)^2$$

$$E_{\overline{xy}} = \frac{\partial \bar{u}}{\partial \bar{y}} + \frac{\partial \bar{v}}{\partial \bar{x}} + \frac{\partial a}{\partial \bar{x}} \frac{\partial a}{\partial \bar{y}} \qquad (3.14)$$

where $\bar{u} = u/\ell$, $\bar{v} = v/\ell$ and u, v are the dimensional in-plane displacements. Before setting up the dynamic equations of in-plane motion we introduce the following consideration:

The frequency of excitation for the electrostatic wall is well below the longitudinal natural frequency of the structure. For this case the in-plane motions are stiffness dominated. Hence, the effect of longitudinal inertia can be neglected.

The above requirement is satisfied if the reduced frequency $fL/c_{sh} \ll 1$ (but a more relaxed criterion can be $\frac{fL}{c_{sh}} < 0.10$), where f is the operating frequency, c_{sh} is the shear wave speed, and L is the wavelength of the primary motion. For the electrostatic model $L = \ell$, the maximum frequency of operation $f = 10$ kHz, and $c_{sh} = \sqrt{\frac{E}{\rho}} = 1690$ m/sec. For the largest wavelength model that we considered, $\ell = 7$ mm. Hence, $\frac{fL}{c_{sh}} = \frac{70}{1690} = 0.04 < 0.1$. Thus the neglect of longitudinal inertia in all the subsequent analysis is well justified.

The dynamic equations of in-plane motion are now given as

$$\frac{\partial \bar{N}_x}{\partial \bar{x}} + \frac{\partial \bar{N}_{xy}}{\partial \bar{y}} = 0$$

$$\frac{\partial \bar{N}_y}{\partial \bar{y}} + \frac{\partial \bar{N}_{xy}}{\partial \bar{x}} = 0 \qquad (3.15)$$

Substituting the relations given in equations (3.13) and (3.14) we get

$$\frac{\partial^2 \bar{u}}{\partial \bar{x}^2} + \frac{1-\nu}{2} \frac{\partial^2 \bar{u}}{\partial y^2} + \frac{1+\nu}{2} \frac{\partial^2 \bar{v}}{\partial \bar{x} \partial \bar{y}} + F_{\bar{x}}(\bar{x}, \bar{y}, \bar{t}) = 0$$

$$\frac{\partial^2 \bar{v}}{\partial \bar{y}^2} + \frac{1-\nu}{2} \frac{\partial^2 \bar{v}}{\partial \bar{x}^2} + \frac{1+\nu}{2} \frac{\partial^2 \bar{u}}{\partial \bar{x} \partial \bar{y}} + F_{\bar{y}}(\bar{x}, \bar{y}, \bar{t}) = 0 \qquad (3.16)$$

where

$$F_{\bar{x}}(\bar{x},\bar{y},\bar{t}) = \frac{\partial a}{\partial \bar{x}}\left[\frac{\partial^2 a}{\partial \bar{x}^2} + \frac{1-\nu}{2}\frac{\partial^2 a}{\partial \bar{y}^2}\right] + \frac{1+\nu}{2}\frac{\partial a}{\partial \bar{y}}\frac{\partial^2 a}{\partial \bar{x}\partial \bar{y}}$$

$$F_{\bar{y}}(\bar{x},\bar{y},\bar{t}) = \frac{\partial a}{\partial \bar{y}}\left[\frac{\partial^2 a}{\partial \bar{y}^2} + \frac{1-\nu}{2}\frac{\partial^2 a}{\partial \bar{x}^2}\right] + \frac{1+\nu}{2}\frac{\partial a}{\partial \bar{x}}\frac{\partial^2 a}{\partial \bar{x}\partial \bar{y}} \tag{3.17}$$

For the deflection shape, we use equation (3.11). Substituting in equation (3.17) we get expressions for $F_{\bar{x}}$ and $F_{\bar{y}}$ as:

$$F_{\bar{x}} = \frac{1}{4}\sum\sum\sum\sum a_{ik}\,a_{j\ell}\left\{\sin\left[(\bar{i}+\bar{j})\bar{x}\right]\cos\left[(\beta_{\bar{k}}+\beta_{\bar{\ell}})\bar{y}\right]\right.$$

$$\cdot\left[\bar{j}\left\{\bar{i}^2 + \frac{1-\nu}{2}\beta_{\bar{k}}^2 + \frac{1+\nu}{2}\beta_{\bar{k}}\,\beta_{\bar{\ell}}\right\}\right] + \sin\left[(\bar{i}-\bar{j})\bar{x}\right]$$

$$\cdot\cos\left[(\beta_{\bar{k}}+\beta_{\bar{\ell}})\bar{y}\right]\left[\bar{j}\left\{\bar{i}^2 + \frac{1-\nu}{2}\beta_{\bar{k}}^2 + \frac{1+\nu}{2}\beta_{\bar{k}}\,\beta_{\bar{\ell}}\right\}\right]$$

$$-\sin\left[(\bar{i}+\bar{j})\bar{x}\right]\cos\left[(\beta_{\bar{k}}-\beta_{\bar{\ell}})\bar{y}\right]\left[\bar{j}\left\{\bar{i}^2 + \frac{1-\nu}{2}\beta_{\bar{k}}^2 - \frac{1+\nu}{2}\beta_{\bar{k}}\,\beta_{\bar{\ell}}\right\}\right]$$

$$-\sin\left[(\bar{i}-\bar{j})\bar{x}\right]\cos\left[(\beta_{\bar{k}}-\beta_{\bar{\ell}})\bar{y}\right]\left[\bar{j}\left\{\bar{i}^2 + \frac{1-\nu}{2}\beta_{\bar{k}}^2 - \frac{1+\nu}{2}\beta_{\bar{k}}\,\beta_{\bar{\ell}}\right\}\right] \tag{3.18}$$

$$F_{\bar{y}} = \frac{1}{4}\sum\sum\sum\sum a_{ik}\,a_{j\ell}\left\{\sin\left[(\beta_{\bar{k}}+\beta_{\bar{\ell}})\bar{y}\right]\cos\left[(\bar{i}+\bar{j})\bar{x}\right]\right.$$

$$\cdot\left[\beta_{\bar{\ell}}(\beta_{\bar{k}}^2 + \frac{1-\nu}{2}\bar{i}^2 + \frac{1+\nu}{2}\bar{i}\,\bar{j})\right] - \sin\left[(\beta_{\bar{k}}+\beta_{\bar{\ell}})\bar{y}\right]\cos\left[(\bar{i}-\bar{j})\bar{x}\right]$$

$$\cdot\left[\beta_{\bar{\ell}}(\beta_{\bar{k}}^2 + \frac{1-\nu}{2}\bar{i}^2 - \frac{1+\nu}{2}\bar{i}\,\bar{j})\right] + \sin\left[(\beta_{\bar{k}}-\beta_{\bar{\ell}})\bar{y}\right]\cos\left[(\bar{i}+\bar{j})\bar{x}\right]$$

$$\cdot\left[\beta_{\bar{\ell}}(\beta_{\bar{k}}^2 + \frac{1-\nu}{2}\bar{i}^2 + \frac{1+\nu}{2}\bar{i}\,\bar{j})\right] - \sin\left[(\beta_{\bar{k}}-\beta_{\bar{\ell}})\bar{y}\right]\cos\left[(\bar{i}-\bar{j})x\right]$$

$$\left.\cdot\left[\beta_{\bar{\ell}}(\beta_{\bar{k}}^2 + \frac{1-\nu}{2}\bar{i}^2 + \frac{1+\nu}{2}\bar{i}\,\bar{j})\right]\right\} \tag{3.19}$$

From the known form of $F_{\bar{x}}$ and $F_{\bar{y}}$ one is now able to proceed to solve $\bar{u}$, $\bar{v}$.

3.4.2. Edge conditions.

The edge conditions describe the state of fixity of the structure for in-plane motions along the edges. For the simply supported periodic structure the edge restraint is

$$u(o,\bar{y},\tau) = u(1,\bar{y},\tau) = 0$$

$$v(\bar{x},o,\tau) = v(x,\frac{b}{\ell},\tau) = 0 \qquad (3.20)$$

3.5. Solution of the In-Plane Motions

Since equations (3.16) are time-dependent equations, a transient solution which depends on the initial condition will exist along with the solution of equations (3.16). This particular solution will be representative of the initial displacement fields that may exist (e.g., if initially the membrane is stretched with uniform tension T, the initial displacement field will be nontrivial).

For the case of zero initial tension, the particular solution takes the trivial form:

$$u_o(\bar{x},\bar{y},\tau) = v_o(\bar{x},\bar{y},\tau) = 0 \qquad (3.21)$$

For the solution of equation 3.16 we take the displacement fields as,

$$\bar{u} = \sum\sum\sum\sum \left[A_{ijk\ell}(\tau) \sin\left\{ (\bar{i} + \bar{j})\bar{x} \right\} \cos\left\{ (\beta_{\bar{k}} + \beta_{\bar{\ell}})\bar{y} \right\} \right.$$

$$+ B_{ijk\ell}(\tau) \sin\left\{ (\bar{i} - \bar{j})\bar{x} \right\} \cos\left\{ (\beta_{\bar{k}} + \beta_{\bar{\ell}})\bar{y} \right\}$$

$$+ C_{ijk\ell}(\tau) \sin\left\{ (\bar{i} + \bar{j})\bar{x} \right\} \cos\left\{ (\beta_{\bar{k}} - \beta_{\bar{\ell}})\bar{y} \right\}$$

$$\left. + D_{ijk\ell}(\tau) \sin\left\{ (\bar{i} - \bar{j})\bar{x} \right\} \cos\left\{ (\beta_{\bar{k}} - \beta_{\bar{\ell}})\bar{y} \right\} \right] \qquad (3.22)$$

$$\bar{v} = \sum\sum\sum\sum \left[E_{ijk\ell}(\tau)\ \cos\left\{(\bar{\bar{i}} + \bar{\bar{j}})\bar{x}\right\} \sin\left\{(\beta_{\bar{k}} + \beta_{\bar{\ell}})\bar{y}\right\} \right.$$

$$+\ F_{ijk\ell}(\tau)\ \cos\left\{(\bar{\bar{i}} - \bar{\bar{j}})\bar{x}\right\} \sin\left\{(\beta_{\bar{k}} + \beta_{\bar{\ell}})\bar{y}\right\}$$

$$+\ G_{ijk\ell}(\tau)\ \cos\left\{(\bar{\bar{i}} + \bar{\bar{j}})\bar{x}\right\} \sin\left\{(\beta_{\bar{k}} - \beta_{\bar{\ell}})\bar{y}\right\}$$

$$+\ H_{ijk\ell}(\tau)\ \cos\left\{(\bar{\bar{i}} - \bar{\bar{j}})\bar{x}\right\} \sin\left\{(\beta_{\bar{k}} - \beta_{\bar{\ell}})\bar{y}\right\} \right] \tag{3.23}$$

Substituting for the derivatives of $\bar{u}$, $\bar{v}$, $F_{\bar{x}}$, $F_{\bar{y}}$ in equation (3.16) and equating like terms one obtains a set of algebraic equations for the coefficients $A_{ijk\ell}$, etc. We give one set of these equations as:

$$A_{ijk\ell}\left[\left(\bar{\bar{i}} + \bar{\bar{j}}\right)^2 + \frac{1 - \nu}{2}\left(\beta_{\bar{k}} + \beta_{\bar{\ell}}\right)^2\right] + E_{ijk\ell}\left[\frac{1 + \nu}{2}\left(\bar{\bar{i}} + \bar{\bar{j}}\right)\left(\beta_{\bar{k}} + \beta_{\bar{\ell}}\right)\right]$$

$$= \frac{1}{4}\ a_{ik}\ a_{j\ell}\left[\bar{\bar{j}}\left\{\bar{\bar{i}}^2 + \frac{1 - \nu}{2}\beta_k^2 + \frac{1 + \nu}{2}\beta_{\bar{k}}\ \beta_{\bar{\ell}}\right\}\right] \tag{3.24}$$

$$A_{ijk\ell}\left[\frac{1 + \nu}{2}\left(\beta_{\bar{k}} + \beta_{\bar{\ell}}\right)\left(\bar{\bar{i}} + \bar{\bar{j}}\right)\right] + E_{ijk\ell}\left[\left(\beta_{\bar{k}} + \beta_{\bar{\ell}}\right)^2 + \frac{1 - \nu}{2}\left(\bar{\bar{i}} + \bar{\bar{j}}\right)^2\right]$$

$$= \frac{1}{4}\ a_{ik}\ a_{j\ell}\left[\beta_{\bar{\ell}}\left\{\beta_k^2 + \frac{1 - \nu}{2}\bar{\bar{i}}^2 + \frac{1 + \nu}{2}\bar{\bar{i}}\ \bar{\bar{j}}\right\}\right] \tag{3.25}$$

and similar equations connecting other coefficients. Finally the coefficients are given as:

$$A_{ijk\ell} = \frac{a_{ik}a_{j\ell}}{2(1 - \nu)}\left[\frac{1}{(\bar{\bar{i}} + \bar{\bar{j}})^2 + (\beta_{\bar{k}} + \beta_{\bar{\ell}})^2}\right]^2$$

$$\cdot\left[\bar{\bar{j}}\left\{\bar{\bar{i}}^2 + \frac{1 - \nu}{2}\beta_k^2 + \frac{1 + \nu}{2}\beta_{\bar{k}}\ \beta_{\bar{\ell}}\right\}\left\{\left(\beta_{\bar{k}} + \beta_{\bar{\ell}}\right)^2 + \frac{1 - \nu}{2}\left(\bar{\bar{i}} + \bar{\bar{j}}\right)^2\right\}\right.$$

$$\left. -\left(\frac{1 + \nu}{2}\right)\left(\bar{\bar{i}} + \bar{\bar{j}}\right)\left(\beta_{\bar{k}} + \beta_{\bar{\ell}}\right)\ \beta_{\bar{\ell}}\left(\beta_k^2 + \frac{1 - \nu}{2}\bar{\bar{i}}^2 + \frac{1 + \nu}{2}\bar{\bar{i}}\ \bar{\bar{j}}\right)\right] \tag{3.26}$$

For $i \neq j$,

$$B_{ijk\ell} = + \frac{a_{ik}a_{j\ell}}{2(1-\nu)} \left[\frac{1}{(\bar{i} - \bar{j})^2 + (\beta_{\bar{k}} + \beta_{\bar{\ell}})^2} \right]^2$$

$$\cdot \bar{j}\left[\bar{i}^2 + \frac{1-\nu}{2}\beta_{\bar{k}}^2 + \frac{1+\nu}{2}\beta_{\bar{k}}\beta_{\bar{\ell}}\right]\left\{\left(\beta_{\bar{k}} + \beta_{\bar{\ell}}\right)^2 + \frac{1-\nu}{2}\left(\bar{i} - \bar{j}\right)^2\right.$$

$$+ \frac{1+\nu}{2}\left(\bar{i} - \bar{j}\right)\left(\beta_{\bar{k}} + \beta_{\bar{\ell}}\right)\beta_{\bar{\ell}}\left(\beta_{\bar{k}}^2 + \frac{1-\nu}{2}\bar{i}^2 - \frac{1+\nu}{2}\bar{i}\,\bar{j}\right)\right] \qquad (3.27)$$

when $i = j$, $B_{ijk\ell} = 0$.

$$C_{ijk\ell} = - \frac{a_{ik}a_{j\ell}}{2(1-\nu)} \left[\frac{1}{(\bar{i} + \bar{j})^2 + (\beta_{\bar{k}} - \beta_{\bar{\ell}})^2} \right]^2$$

$$\cdot \left\{\bar{j}\left[\bar{i}^2 + \frac{1-\nu}{2}\beta_{\bar{k}}^2 - \frac{1+\nu}{2}\beta_{\bar{k}}\beta_{\bar{\ell}}\right]\left[\left(\beta_{\bar{k}} - \beta_{\bar{\ell}}\right)^2 + \frac{1-\nu}{2}\left(\bar{i} + \bar{j}\right)^2\right]\right.$$

$$+ \frac{1+\nu}{2}\left(\bar{i} + \bar{j}\right)\left(\beta_{\bar{k}} - \beta_{\bar{\ell}}\right)\beta_{\bar{\ell}}\left(\beta_{\bar{k}}^2 + \frac{1-\nu}{2}\bar{i}^2 + \frac{1+\nu}{2}\bar{i}\,\bar{j}\right)\right\} \qquad (3.28)$$

and whenever $i = j$, $D_{ijk\ell} = 0$, and in other cases

$$D_{ijk\ell} = - \frac{a_{ik}a_{j\ell}}{2(1-\nu)} \left[\frac{1}{(\bar{i} - \bar{j})^2 + (\beta_{\bar{k}} - \beta_{\bar{\ell}})^2} \right]^2$$

$$\cdot \left[\bar{j}\left(\bar{i}^2 + \frac{1-\nu}{2}\beta_{\bar{k}}^2 - \frac{1+\nu}{2}\beta_{\bar{k}}\beta_{\bar{\ell}}\right)\left(\overline{\beta_{\bar{k}} + \beta_{\bar{\ell}}}^2 + \frac{1-\nu}{2}\overline{\bar{i} - \bar{j}}^2\right)\right.$$

$$- \frac{1+\nu}{2}\left(\bar{i} - \bar{j}\right)\beta_{\bar{\ell}}\left(\beta_{\bar{k}} - \beta_{\bar{\ell}}\right)\left(\beta_{\bar{k}}^2 + \frac{1-\nu}{2}\bar{i}^2 - \frac{1+\nu}{2}\bar{i}\,\bar{j}\right)\right] \qquad (3.29)$$

15

$$E_{ijk\ell} = -\frac{a_{ik}a_{j\ell}}{2(1-\nu)}\left[\frac{1}{(\bar{\imath}+\bar{\jmath})^2 + (\beta_{\bar{k}} + \beta_{\bar{\ell}})^2}\right]^2$$

$$\cdot\left[\frac{1+\nu}{2}\left(\beta_{\bar{k}} + \beta_{\bar{\ell}}\right)\left(\bar{\imath}+\bar{\jmath}\right)\bar{\jmath}\left\{\bar{\imath}^2 + \frac{1-\nu}{2}\beta_{\bar{k}}^2 + \frac{1+\nu}{2}\beta_{\bar{k}}\beta_{\bar{\ell}}\right\}\right.$$

$$\left.\cdot\left\{\left(\bar{\imath}+\bar{\jmath}\right)^2 + \frac{1-\nu}{2}\left(\beta_{\bar{k}} + \beta_{\bar{\ell}}\right)^2\right\}\left\{\beta_{\bar{k}}^2 + \frac{1-\nu}{2}\bar{\imath}^2 + \frac{1+\nu}{2}\bar{\imath}\,\bar{\jmath}\right\}\beta_{\bar{\ell}}\right] \quad (3.30)$$

$$F_{ijk\ell} = -\frac{a_{ik}a_{j\ell}}{2(1-\nu)}\left[\frac{1}{(\bar{\imath}-\bar{\jmath})^2 + (\beta_{\bar{k}} + \beta_{\bar{\ell}})^2}\right]^2$$

$$\cdot\left\{\frac{1+\nu}{2}\left(\beta_{\bar{k}} + \beta_{\bar{\ell}}\right)\left(\bar{\imath}-\bar{\jmath}\right)\bar{\jmath}\left[\bar{\imath}^2 + \frac{1-\nu}{2}\beta_{\bar{k}}^2 + \frac{1+\nu}{2}\beta_{\bar{k}}\beta_{\bar{\ell}}\right]\right.$$

$$\left. + \left[\left(\bar{\imath}-\bar{\jmath}\right)^2 + \frac{1-\nu}{2}\left(\beta_{\bar{k}} + \beta_{\bar{\ell}}\right)^2\right]\left[\beta_{\bar{k}}^2 + \frac{1-\nu}{2}\bar{\imath}^2 - \frac{1+\nu}{2}\bar{\imath}\,\bar{\jmath}\right]\beta_{\bar{\ell}}\right\} \quad (3.31)$$

$G_{ijk\ell} = 0$ for $k = \ell$ and

$$G_{ijk\ell} = \frac{a_{ik}a_{j\ell}}{2(1-\nu)}\left[\frac{1}{(\bar{\imath}+\bar{\jmath})^2 + (\beta_{\bar{k}} - \beta_{\bar{\ell}})^2}\right]^2$$

$$\cdot\left\{\frac{1+\nu}{2}\left(\beta_{\bar{k}} - \beta_{\bar{\ell}}\right)\left(\bar{\imath}+\bar{\jmath}\right)\bar{\jmath}\left[\bar{\imath}^2 + \frac{1-\nu}{2}\beta_{\bar{k}}^2 - \frac{1+\nu}{2}\beta_{\bar{k}}\beta_{\bar{\ell}}\right]\right.$$

$$\left. + \beta_{\bar{\ell}}\left[\left(\bar{\imath}+\bar{\jmath}\right)^2 + \frac{1-\nu}{2}\left(\beta_{\bar{k}} - \beta_{\bar{\ell}}\right)^2\right]\left[\beta_{\bar{k}}^2 + \frac{1-\nu}{2}\bar{\imath}^2 + \frac{1+\nu}{2}\bar{\imath}\,\bar{\jmath}\right]\right\} \quad (3.32)$$

and $H_{ijk\ell} \equiv 0$ if $k = \ell$ or else

$$H_{ijk\ell} = \frac{a_{ik}a_{j\ell}}{2(1-\nu)}\left[\frac{1}{(\bar{\imath}-\bar{\jmath})^2 + (\beta_{\bar{k}} - \beta_{\bar{\ell}})^2}\right]^2$$

$$\cdot\left\{\frac{1+\nu}{2}\left(\beta_{\bar{k}} - \beta_{\bar{\ell}}\right)\left(\bar{\imath}-\bar{\jmath}\right)\bar{\jmath}\left[\bar{\imath}^2 + \frac{1-\nu}{2}\beta_{\bar{k}}^2 - \frac{1+\nu}{2}\beta_{\bar{k}}\beta_{\bar{\ell}}\right]\right.$$

$$\left. - \beta_{\bar{\ell}}\left[\left(\bar{\imath}-\bar{\jmath}\right)^2 + \left(\beta_{\bar{k}} - \beta_{\bar{\ell}}\right)^2\left(\frac{1-\nu}{2}\right)\right]\left[\beta_{\bar{k}}^2 + \frac{1-\nu}{2}\bar{\imath}^2 - \frac{1+\nu}{2}\bar{\imath}\,\bar{\jmath}\right]\right\} \quad (3.33)$$

16

Having obtained the coefficients one is now able to evaluate the midplane forces through the help of equations (3.13) and (3.14). Thus

$$\bar{N}_x = \frac{1}{(1-\nu^2)} \sum\sum\sum\sum \left[\left\{ A_{ijk\ell} \left(\bar{i} + \bar{j}\right) + \nu E_{ijk\ell} \left(\beta_{\bar{k}} + \beta_{\bar{\ell}}\right) \right. \right.$$

$$\left. - \frac{a_{ik} a_{j\ell}}{8} \left(\bar{i}\,\bar{j} + \nu\,\beta_{\bar{k}}\,\beta_{\bar{\ell}}\right) \right\} \cos\left(\bar{i} + \bar{j}\right)\bar{x} \, \cos\left(\beta_{\bar{k}} + \beta_{\bar{\ell}}\right)\bar{y}$$

$$+ \left\{ B_{ijk\ell} \left(\bar{i} - \bar{j}\right) + \nu F_{ijk\ell} \left(\beta_{\bar{k}} + \beta_{\bar{\ell}}\right) - \frac{a_{ik} a_{j\ell}}{8} \left(\bar{i}\,\bar{j} - \nu\,\beta_{\bar{k}}\,\beta_{\bar{\ell}}\right) \right\}$$

$$\cdot \cos\left(\bar{i} - \bar{j}\right)\bar{x} \, \cos\left(\beta_{\bar{k}} + \beta_{\bar{\ell}}\right)\bar{y}$$

$$+ \left\{ C_{ijk\ell} \left(\bar{i} + \bar{j}\right) + \nu G_{ijk\ell} \left(\beta_{\bar{k}} - \beta_{\bar{\ell}}\right) + \frac{a_{ik} a_{j\ell}}{8} \left(\bar{i}\,\bar{j} - \nu\,\beta_{\bar{k}}\,\beta_{\bar{\ell}}\right) \right\}$$

$$\cdot \cos\left(\bar{i} + \bar{j}\right)\bar{x} \, \cos\left(\beta_{\bar{k}} - \beta_{\bar{\ell}}\right)\bar{y} + \left\{ \cos\left(\bar{i} - \bar{j}\right)\bar{x} \, \cos\left(\beta_{\bar{k}} - \beta_{\bar{\ell}}\right)\bar{y} \right\}$$

$$+ \left\{ D_{ijk\ell} \left(\bar{i} - \bar{j}\right) + \nu H_{ijk\ell} \left(\beta_{\bar{k}} - \beta_{\bar{\ell}}\right) + \frac{a_{ik} a_{j\ell}}{8} \left(\bar{i}\,\bar{j} + \nu\,\beta_{\bar{k}}\,\beta_{\bar{\ell}}\right) \right\} \tag{3.34}$$

$$\bar{N}_y = \frac{1}{(1-\nu^2)} \sum\sum\sum\sum \left[\left\{ \nu A_{ijk\ell} \left(\bar{i} + \bar{j}\right) + E_{ijk\ell} \left(\beta_{\bar{k}} + \beta_{\bar{\ell}}\right) \right. \right.$$

$$\left. - \frac{a_{ik} a_{j\ell}}{8} \left(\beta_{\bar{k}}\,\beta_{\bar{\ell}} + \nu\,\bar{i}\,\bar{j}\right) \right\} \cos\left(\bar{i} + \bar{j}\right)\bar{x} \, \cos\left(\beta_{\bar{k}} + \beta_{\bar{\ell}}\right)\bar{y}$$

$$+ \left\{ \nu B_{ijk\ell} \left(\bar{i} - \bar{j}\right) + F_{ijk\ell} \left(\beta_{\bar{k}} + \beta_{\bar{\ell}}\right) + \frac{a_{ik} a_{j\ell}}{8} \left(\beta_k\,\beta_\ell - \bar{i}\,\bar{j}\,\nu\right) \right\}$$

$$\cdot \cos\left(\bar{i} - \bar{j}\right)\bar{x} \, \cos\left(\beta_{\bar{k}} + \beta_{\bar{\ell}}\right)\bar{y} + \left\{ \nu C_{ijk\ell} \left(\bar{i} + \bar{j}\right) + G_{ijk\ell} \left(\beta_{\bar{k}} - \beta_{\bar{\ell}}\right) \right.$$

$$+ \frac{a_{ik} a_{j\ell}}{8} \left[\nu\,\bar{i}\,\bar{j} - \beta_{\bar{k}}\,\beta_{\bar{\ell}}\right] \right\} \cos\left(\bar{i} + \bar{j}\right)\bar{x} \, \cos\left(\beta_{\bar{k}} - \beta_{\bar{\ell}}\right)\bar{y} \tag{3.35}$$

(cont'd)

$$+\left\{\nu\, D_{ijk\ell}\left(\bar{i}-\bar{j}\right)+H_{ijk\ell}\left(\beta_{\bar{k}}-\beta_{\bar{\ell}}\right)+\frac{a_{ik}a_{j\ell}}{8}\left[\nu\,\bar{i}\,\bar{j}+\beta_{\bar{k}}\,\beta_{\bar{\ell}}\right]\right\}$$

$$\cdot\,\cos\left(\bar{i}-\bar{j}\right)\bar{x}\,\cos\left(\beta_{\bar{k}}-\beta_{\bar{\ell}}\right)\bar{y}\Bigg]\qquad(3.35)$$

and

$$\bar{N}_{xy}=\frac{1}{2(1+\nu)}\sum\sum\sum\sum\left[\left\{\frac{a_{ik}a_{j\ell}}{4}\left(\beta_{\bar{k}}\,\bar{j}\right)-A_{ijk\ell}\left(\beta_{\bar{k}}+\beta_{\bar{\ell}}\right)\right.\right.$$

$$\left.-\,E_{ijk\ell}\left(\bar{i}+\bar{j}\right)\right\}\sin\left(\bar{i}+\bar{j}\right)\bar{x}\,\sin\left(\beta_{\bar{k}}+\beta_{\bar{\ell}}\right)\bar{y}$$

$$\cdot\left\{B_{ijk\ell}\left(\beta_{\bar{k}}+\beta_{\bar{\ell}}\right)+F_{ijk\ell}\left(\bar{i}-\bar{j}\right)+\frac{a_{ik}a_{j\ell}}{4}\,\beta_{\bar{k}}\,\bar{j}\right\}\sin\left(\bar{i}-\bar{j}\right)\bar{x}$$

$$\cdot\,\sin\left(\beta_{\bar{k}}+\beta_{\bar{\ell}}\right)\bar{y}+\left\{-\,C_{ijk\ell}\left(\beta_{\bar{k}}-\beta_{\bar{\ell}}\right)-G_{ijk\ell}\left(\bar{i}+\bar{j}\right)\right.$$

$$\left.+\,\frac{a_{ik}a_{j\ell}}{4}\,\beta_{\bar{k}}\,\bar{j}\right\}\sin\left(\bar{i}+\bar{j}\right)\bar{x}\,\sin\left(\beta_{\bar{k}}-\beta_{\bar{\ell}}\right)\bar{y}-\left\{D_{ijk\ell}\left(\beta_{\bar{k}}-\beta_{\bar{\ell}}\right)\right.$$

$$\left.\left.+\,H_{ijk\ell}\left(\bar{i}-\bar{j}\right)+\frac{a_{ik}a_{j\ell}}{4}\,\beta_{\bar{k}}\,\bar{j}\right\}\sin\left(\bar{i}-\bar{j}\right)\bar{x}\,\sin\left(\beta_{\bar{k}}-\beta_{\bar{\ell}}\right)\bar{y}\right]\qquad(3.36)$$

Having obtained the terms $\bar{N}_{x}$, $\bar{N}_{y}$, $\bar{N}_{xy}$ one can now solve equation (3.1).

3.6. Solution of the Transverse Motion

The governing equation (3.3) can be solved as modal equations in time. The form of a is given by equation (3.11) as:

$$a=\sum_{m}\sum_{n}a_{mn}\,\sin\bar{m}\,\bar{x}\,\sin(\beta\bar{n}\,\bar{y})$$

The Raleigh-Ritz approximation to equation (3.3) is obtained by multiplying equation (3.3) by $\sin\bar{p}\,\bar{x}\,\sin\beta_{\bar{q}}\,\bar{y}$ and integrating over the x - y space.

Defining:

$$A_{ijk\ell}^{(1)} = \left[\left(\bar{i} + \bar{j}\right) A_{ijk\ell} + \nu\, E_{ijk\ell}\, \left(\beta_{\bar{k}} + \beta_{\bar{\ell}}\right) - \frac{a_{ik}a_{j\ell}}{8}\left(\bar{i}\,\bar{j} + \nu\, \beta_{\bar{k}}\, \beta_{\bar{\ell}}\right)\right] \qquad (3.37)$$

$$A_{ijk\ell}^{(2)} = \left[B_{ijk\ell}\left(\bar{i} - \bar{j}\right) + \nu\, F_{ijk\ell}\left(\beta_{\bar{k}} + \beta_{\bar{\ell}}\right) - \frac{a_{ik}a_{j\ell}}{8}\left(\bar{i}\,\bar{j} - \nu\, \beta_{\bar{k}}\, \beta_{\bar{\ell}}\right)\right] \qquad (3.38)$$

$$A_{ijk\ell}^{(3)} = \left[C_{ijk\ell}\left(\bar{i} + \bar{j}\right) + \nu\, G_{ijk\ell}\left(\beta_{\bar{k}} - \beta_{\bar{\ell}}\right) + \frac{a_{ik}a_{j\ell}}{8}\left(\bar{i}\,\bar{j} - \nu\, \beta_{\bar{k}}\, \beta_{\bar{\ell}}\right)\right] \qquad (3.39)$$

$$A_{ijk\ell}^{(4)} = \left[D_{ijk\ell}\left(\bar{i} - \bar{j}\right) + \nu\, H_{ijk\ell}\left(\beta_{\bar{k}} - \beta_{\bar{\ell}}\right) + \frac{a_{ik}a_{j\ell}}{8}\left(\bar{i}\,\bar{j} - \nu\, \beta_{\bar{k}}\, \beta_{\bar{\ell}}\right)\right] \qquad (3.40)$$

and

$$B_{ijk\ell}^{(1)} = \nu\, A_{ijk\ell}\left(\bar{i} + \bar{j}\right) + E_{ijk\ell}\left(\beta_{\bar{k}} + \beta_{\bar{\ell}}\right) - \frac{a_{ik}a_{j\ell}}{8}\left(\beta_{\bar{k}}\, \beta_{\bar{\ell}} + \nu\, \bar{i}\,\bar{j}\right) \qquad (3.41)$$

$$B_{ijk\ell}^{(2)} = \nu\, B_{ijk\ell}\left(\bar{i} - \bar{j}\right) + F_{ijk\ell}\left(\beta_{\bar{k}} + \beta_{\bar{\ell}}\right) + \frac{a_{ik}a_{j\ell}}{8}\left(\beta_{\bar{k}}\, \beta_{\bar{\ell}} - \bar{i}\,\bar{j}\,\nu\right) \qquad (3.42)$$

$$B_{ijk\ell}^{(3)} = \nu\, C_{ijk\ell}\left(\bar{i} + \bar{j}\right) + G_{ijk\ell}\left(\beta_{\bar{k}} - \beta_{\bar{\ell}}\right) + \frac{a_{ik}a_{j\ell}}{8}\left(\nu\, \bar{i}\,\bar{j} - \beta_{\bar{k}}\, \beta_{\bar{\ell}}\right) \qquad (3.43)$$

$$B_{ijk\ell}^{(4)} = \nu\, D_{ijk\ell}\left(\bar{i} - \bar{j}\right) + H_{ijk\ell}\left(\beta_{\bar{k}} - \beta_{\bar{\ell}}\right) + \frac{a_{ik}a_{j\ell}}{8}\left(\nu\, \bar{i}\,\bar{j} + \beta_{\bar{k}}\, \beta_{\bar{\ell}}\right) \qquad (3.44)$$

and

$$C_{ijk\ell}^{(1)} = \frac{1}{4}\, a_{ik}a_{j\ell}\, \beta_{\bar{k}}\, \bar{j} - A_{ijk\ell}\left(\beta_{\bar{k}} + \beta_{\bar{\ell}}\right) - E_{ijk\ell}\left(\bar{i} + \bar{j}\right) \qquad (3.45)$$

$$C_{ijk}^{(2)} = -\left[B_{ijk\ell}\left(\beta_{\bar{k}} + \beta_{\bar{\ell}}\right) + F_{ijk\ell}\left(\bar{i} - \bar{j}\right) + \frac{a_{ik}a_{j\ell}}{8}\, \beta_{\bar{k}}\, \bar{j}\right] \qquad (3.46)$$

19

$$C_{ijk\ell}^{(3)} = -C_{ijk\ell} \left(\beta_{\overline{k}} - \beta_{\overline{\ell}} \right) - G_{ijk\ell} \left(\overline{i} + \overline{j} \right) + \frac{a_{ik}a_{j\ell}}{4} \beta_{\overleftarrow{k}} \overline{j} \tag{3.47}$$

and

$$C_{ijk\ell}^{(4)} = - \left[D_{ijk\ell} \left(\beta_{\overline{k}} - \beta_{\overline{\ell}} \right) + H_{ijk\ell} \left(\overline{i} - \overline{j} \right) + \frac{a_{ik}a_{j\ell}}{4} \beta_{\overline{k}} \overline{j} \right] \tag{3.48}$$

and also the following parameters

$$R_1 = i + j + p$$

$$R_2 = i + j + r$$

$$R_3 = i + j - p$$

$$R_4 = i + p - j$$

$$R_5 = i + r - j$$

$$R_6 = i + p + r$$

$$R_7 = j + p + r \tag{3.49}$$

and

$$S_1 = k + \ell + q$$

$$S_2 = k + \ell + s$$

$$S_3 = k + s + q$$

$$S_4 = \ell + s + q$$

$$S_5 = k + \ell - q \tag{3.50}$$

(cont'd)

$$S_6 = k - \ell + s$$

$$S_7 = k - s + q \qquad\qquad\qquad (3.50)$$

<div align="right">(concl'd)</div>

and the Kronecker delta function

$$\delta_{rs} = 0 \qquad r \neq s$$

$$\delta_{rs} = 1 \qquad r = 1 \qquad\qquad\qquad (3.51)$$

the Rayleigh-Ritz approximation equation (3.3) is then

$$\frac{d^2 a_{pq}}{d\tau^2} + K_{pq} \, a_{pq} + \sum_i \sum_j \sum_k \sum_\ell \sum_r \sum_s \frac{1}{4(1 - \nu^2)} \, a_{pq} \left[a_{ik} a_{j\ell} \right]$$

$$\cdot \left[\delta_1 \, P_1 + \delta_2 \, P_2 + \delta_3 \, P_3 + \delta_4 \, P_4 \right] = P_{Gen}^{pq} \qquad\qquad (3.52)$$

where

$$K_{pq} = \frac{\gamma^2}{12(1 - \nu^2)} \left(\bar{p}^2 + \beta_q^2 \right)^2 \qquad\qquad\qquad (3.53)$$

$$P_1 = \frac{1}{a_{ij} a_{k\ell}} \left[\bar{p}^2 \, A_{ijk\ell}^{(1)} + \beta_q^2 \, \beta_{ijk\ell}^{(1)} \right]$$

$$P_2 = \frac{1}{a_{ij} a_{k\ell}} \left[\bar{p}^2 \, A_{ijk\ell}^{(2)} + \beta_q^2 \, \beta_{ijk\ell}^{(2)} \right]$$

$$P_3 = \frac{1}{a_{ij} a_{k\ell}} \left[\bar{p}^2 \, A_{ijk\ell}^{(3)} + \beta_q^2 \, \beta_{ijk\ell}^{(3)} \right]$$

$$P_4 = \frac{1}{a_{ij} a_{k\ell}} \left[\bar{p}^2 \, A_{ijk\ell}^{(4)} + \beta_q^2 \, \beta_{ijk\ell}^{(4)} \right] \qquad\qquad (3.54)$$

and

<div align="right">21</div>

$$\delta_1 = \left(\delta_{R1r} + \delta_{R2p} - \delta_{R3r}\right)\left(\delta_{S1s} + \delta_{S2q} - \delta_{S5s}\right)$$

$$\delta_2 = \left(\delta_{S1s} + \delta_{S2q} - \delta_{S5s}\right)\left(\delta_{R4r} + \delta_{R5p} - \delta_{R6j} - \delta_{R7i}\right)$$

$$\delta_3 = \left(\delta_{R1r} + \delta_{R2p} - \delta_{R3r}\right)\left(\delta_{S7\ell} + \delta_{S6q} - \delta_{S3\ell} - \delta_{S4k}\right)$$

$$\delta_4 = \left(\delta_{R4r} + \delta_{R5p} - \delta_{R6j} - \delta_{R7i}\right)\left(\delta_{S7\ell} + \delta_{S6q} - \delta_{S3\ell} - \delta_{S4k}\right) \tag{3.55}$$

and

$$P_{Gen}^{pq} = 4\beta \left[\int_0^{\frac{1}{\beta}} \int_0^1 \bar{P}_e\ (\bar{x},\bar{y})\ \sin\ (\bar{p}\ \bar{x})\ \sin\ (\beta_{\bar{q}}\ \bar{y})\ d_{\bar{x}}\ d_{\bar{y}} \right] \tag{3.56}$$

The set of ordinary differential equations is highly nonlinear because of the presence of terms such as $a_{ij}a_{k\ell}\ a_{pq}$. The coupled set of such equations can be solved using numerical techniques. Analytical solutions might be impossible except in the simplest case, e.g. a one mode solution such as $i = j = k = \ell = p = q = 1$. When the electrostatic wall model is subjected to fluidic forces such as will occur if used for drag reduction studies, a complete analysis of the problem as formulated above with a few normal modes in the deflection shape might be necessary. This is especially so in flutter regimes of structural motion. In such cases the generalized loading will consist of three main contributions: (a) random turbulent pressure loading which can be insignificant unless flow speeds are fairly large and the membrane thickness very small; (b) wall pressure loading due to the interaction of a pulsating boundary in a turbulent boundary layer flow; the magnitude of this loading can be significant under a variety of circumstances including the flutter mode instability case; and (c) the electrostatic wall loading due to the primary excitation through electrostatic attraction forces.

In an actual experiment with flow over the structure such as in a windtunnel other loadings might also be present. The most common of these are pressure gradients in the tunnel and static pressure differentials across the membrane. An accurate prediction of the structural response depends largely on identifying all these influences.

4. ANALYSIS OF THE ELECTRIC FIELD

4.1. Determination of the Primary Electric Field

The schematic of the electrostatic system is shown in figure 1a. The output from the transformer T is biased at the center tap and connected to terminals A and B as indicated. An array of electrodes which is etched on a printed circuit board and coated by degassed epoxy cement or lacquer forms one part of the electrostatic wall system. A grounded conducting sheet (membrane) which is structurally supported periodically at distances "ℓ" apart and separated from the electrodes at a height "H" forms with these electrodes a capacitive network. The membrane is free to move transversely; when alternate electrodes are connected to the terminals A and B respectively the membrane is subjected to an electrostatic force distribution and deflects under these forces. The space between the membrane and the electrodes is filled with air and sealed. To obtain maximum force for given terminal voltages, the distance between the membrane and the electrodes should be as small as possible. However, as the distance between the membrane and the electrodes becomes smaller and smaller the applied voltages in the terminals must be reduced lest a breakdown of the electrostatic wall system due to arcing will occur. The breakdown potential for a given separation in air is given by Paschen's law. For air at NTP the breakdown rms potential gradient is 3.1 kV/mm. If instead of air a fluid such as SF_6 is used, the breakdown voltage gradient can be raised by a factor of two.

In figure 2 we show a typical bay of the electrostatic wall configuration. The electric field between the electrodes and the membrane can be obtained by solving in the domain

$$\nabla^2 V = 0 \tag{4.1}$$

with the boundary conditions (as indicated in fig. 2).

$$
\begin{aligned}
z &= 0 & V &= 0 \\
z &= H & V &= V_0 + \bar{V}_1(x,H)\ \sin \Omega t \\
x &= 0, \ell & V &= V_0\, z/H
\end{aligned}
\tag{4.2}
$$

In figure 3, $\bar{V}_1(x,H)$ and its Fourier series representation is shown. From the figure it can be seen that

$$\bar{V}_1(x,H) \doteq 1.1463 \, V_1 \, \sin 2\pi\frac{x}{\ell} \, \sin \Omega t \qquad (4.3)$$

is a good approximation.

The solution of equation (4.1) with the boundary conditions given in equation (4.2) is rather straightforward and can be written as

$$V = \frac{V_o Z}{H} + 1.1463 \, V_1 \, \sin \frac{2\pi x}{\ell} \, \sin \Omega t \left[\frac{\sinh\left(2\pi\frac{z}{\ell}\right)}{\sinh 2\pi \frac{H}{\ell}} \right] \qquad (4.4)$$

The electric field in the dielectric between the electrodes and the membrane is thus

$$E_x = E_y = o$$

$$E_z = \frac{V_o}{H} + 7.2024 \, \frac{V_1}{\ell} \, \sin \frac{2\pi x}{\ell} \, \sin \Omega t \, \frac{\cosh\left[\frac{2\pi z}{\ell}\right]}{\sinh\left(\frac{2\pi H}{\ell}\right)} \qquad (4.5)$$

Force density due to primary field. The membrane is subjected to a force

$$P_o^e = \frac{\varepsilon E_z^{\,2}}{2} \Big|_{z=0} \qquad (4.6)$$

Thus the generalized electrostatic force is

$$P_{Gen}^{pq} = 0 \quad \text{for } p > 1$$

and for P = 1

$$P_{Gen}^{pq} = \frac{1}{\left(2q - 1\right)\sinh\left(\frac{2\pi H}{\ell}\right)} \left[\frac{0.935 \, \varepsilon \, V_o \, V_1}{E\gamma H\ell} \right] \sin \omega \, \tau \qquad (4.7)$$

Optimal values for V_0, V_1. There is a limit to the maximum voltages V_0, V_1 permissible for a given configuration, which is determined by the rms voltage gradient to be less than the breakdown value (3.1 kV/mm for air at NTP).

From equation (4.5) the maximum rms electric field value is given as

$$\text{rms value} = \sqrt{\left(\frac{V_o}{H}\right)^2 + \frac{1}{2}\left(\frac{V_1}{\ell}\coth\left(\frac{2\pi H}{\ell}\right)7.2024\right)^2}$$

$$\leq 3.1 \text{ Mv/m} \tag{4.8}$$

In order to obtain the optimal values of V_0, V_1 for maximum generalized forces, one must minimize the generalized forces subject to the constraint equation (4.8).

4.2. Requirements, Ratings, etc. of the Electrical Networks for Electrostatic Wall Configuration

In figure 4a is shown the schematic of the electrical setup. Power is drawn from a signal generator stepped through a power amplifier and fed into a transformer. The transformer output is fed into the exciter for the electrostatic configuration. Basically the electrostatic wall comprising the membrane and the terminals act as a capacitive load. The capacitance can be measured using a capacity meter available commercially. It is also fairly straightforward to theoretically model this electrostatic wall as a discrete capacitive network and evaluate the capacitances of the wall as done in reference 6.

For satisfactory performance of the electrostatic wall system the following points should be kept in mind:

(i) The electrostatic wall should be operated below the breakdown voltage levels to avoid arcing and sparking and consequent degradation of the terminals and burnout or charring of the membrane surface.

(ii) Collapse of the membrane into the cavity and consequent shorting of the electrical system should at all costs be avoided lest the transformer or power amplifier be damaged.

(iii) Any L-C oscillation due to the loading of the system should be avoided. This is accomplished by designing the outages of the units such that the external load is well within the operating load for the system.

4.3. Evaluation of the Maximum Permissible Capacitive
Load for the Electrical System

The ratings of the transformer are

Turns ratio $a = N_2/N_1 = 40$

Resistance on the primary side $R_1 = 0.5\ \Omega$

Inductive reactance on the primary side $X_1 = 8\ \Omega$ @ 1 kHz

Resistance on the secondary side $R_2 = 2\ k\Omega$

Inductive reactance on the secondary side $X_2 = 50\ k\Omega$ @ 1 kHz

External load is capacitive with a reactance X_c @ 1 kHz $= \dfrac{1}{j\omega C}$

In figure 4b the equivalent circuit is shown. It is assumed that the magnetizing current is zero, an assumption which is quite valid (usually it is 5 to 10 percent of the primary current). With this assumption the reactance $X_{mag} = \infty$.

From figure 4:

The equivalent impedance on the primary side = Zeq

$$= j\ X_{L_1} + R_1 + j\ \frac{X_{L_2}}{a^2} + \frac{R_2}{a^2} + \frac{1}{j\omega Ca^2}$$

$$= \left(X_{L_1} + \frac{X_{L_2}}{a^2} - \frac{1}{\omega Ca^2}\right)j - \left(R_1 + \frac{R_2}{a^2}\right)$$

$$= \bar{z}_{\angle}\theta \tag{4.9}$$

The primary current
$$I_1 = V/z_{eq} = \frac{V}{z}\ {\angle}{-\theta} \tag{4.10}$$

The load current
$$I_2 = I_1/a = \frac{V}{za}\ {\angle}{-\theta} \tag{4.11}$$

The circuit becomes a resonant circuit when the reactance is zero,

i.e.
$$X_{L_1} + X_{L_2} = \frac{1}{\omega Ca^2} \tag{4.12}$$

The operating range of the electrostatic wall for experiments lies between 200 Hz to 2 kHz. In order to protect the power amplifier the resonant frequency

which can be determined from equation (4.12) should be well above this range. Fixing the resonant frequency f to be around 3000 Hz we obtain the condition that capacitance of the electrostatic wall be

$$c < \frac{1}{2\pi f \left[\dfrac{x_1 f}{1000} a^2 + \dfrac{x_2 f}{1000} \right]} = \underline{\underline{280 \text{ pf}}}$$

With a proper choice of equipment (i.e. low reactance transformers and power amplifiers), the size and capacity of the electrostatic wall can be enhanced considerably for the same range of operating frequencies. The foregoing discussion makes it imperative that when different models require laboratory testing the capacitance of the model be measured to see whether there is any limitation on operating frequency imposed by the choice and availability of power equipments.

5. THEORETICAL ANALYSIS AND EXPERIMENTAL VERIFICATION OF THE PERFORMANCE OF THE ELECTROSTATIC WALL

5.1. Analysis of Structural Motion

We consider the case where the generalized force is due primarily to the electrostatic field set up in the model. The structural motion resulting can be studied by solving equation (3.52) with the expression for P_{Gen}^{pq} provided by equation (4.7). The deflection shape a is given in equation (3.11) as

$$a = \sum_m \sum_n a_{mn} \sin \bar{m} \bar{x} \sin \beta \frac{\bar{n}}{n} \bar{y}$$

We consider the case where $\beta = \ell/b \ll 1$, corresponding to the situation of the width of the bays $b \simeq 50 \ell$ which was true for most of the wall to be built for tunnel testing.

From the nature of the generalized load P_{Gen}^{pq} given in equation (4.7), i.e.

$$\begin{aligned} P_{Gen}^{pq} &= 0 \quad p > 1 \\ &= F(q) \quad p = 1 \end{aligned}$$

27

it is obvious that the deflection shape can be approximated as

$$a = \sum_n a_m \sin 2\pi\bar{x} \sin \beta\frac{}{n} \bar{y} \tag{5.1}$$

It is not at once clear how far the summation implied in equation (5.1) must be carried out. However, the nature of the generalized forces P^{pq}_{Gen} (being proportional to $\frac{1}{(2q-1)}$) suggests that at best the first two modes are important.

The equation system for two mode series is of the form

$$\frac{d^2 a_{11}}{d\tau^2} + a_{11}\left[k_{11}\right] + G^1_{11} a^3_{11} + G^1_{12} a^2_{11} a_{12} + G^1_{13} a_{11} a^2_{12} = P^{11}_{Gen}$$

$$\frac{d^2 a_2}{d\tau^2} + a_{22}\left[k_{22}\right] + G^1_{22} a^3_{12} + G^1_{21} a^2_{11} a_{12} + G^1_{23} a_{11} a^2_{12} = P^{12}_{Gen} \tag{5.2}$$

In table 1 the coefficients G^1_{11}, G^1_{12}, G^1_{13}, k_{11}, etc. are all tabulated for arbitrary β, using a program called MACSYMA available through ARPA, NBS or MIT network.

5.1.1. _Initial approximations._ - We shall examine the case of $\beta \ll 1$ and assume that the percentage of the second normal mode in the solution to the problem is entirely insignificant in order to obtain an idea of the sensitivity of the solution to truncation of the series. Setting $\beta = 0$ and taking only the first of the equation set in equation (5.2) one obtains

$$\frac{d^2 a_{11}}{d\tau^2} + k_{11} a_{11} + G^1_{11} a^3_{11} = P^{11}_{Gen} \tag{5.3}$$

From equation (4.7) $P^{11}_{Gen} = P_{10} \sin \Omega\tau$ (5.4a)

where $P_{10} = \dfrac{1}{\sinh \frac{2\pi H}{\ell}}\left[\dfrac{0.935 \, \varepsilon \, V_0 \, V_1}{E\gamma H\ell}\right]$ (5.4b)

Then terms k_{11} and G^1_{11} in equation (5.3) have (for $\beta = 0$) values

$$k_{11} = \frac{16\pi^4\gamma^2}{12(1 - \nu^2)} \quad , \quad G_{11}^1 = \frac{(3 - \nu^2)\pi^4}{(1 - \nu^2)}$$

<div align="right">(5.4c)</div>

Equation (5.3) can be rewritten using the following transformation:

$$\theta = \frac{\pi}{2} - \Omega\,\tau, \quad u = a_{11}\sqrt{\frac{G_{11}^1}{\Omega}} \quad , \quad \beta_1 = \frac{k_{11}}{\Omega^2}$$

and $\qquad P_2 = P_{10}\sqrt{\dfrac{G_{11}^1}{\Omega^3}}$

<div align="right">(5.5)</div>

as

$$\frac{d^2u}{d\theta^2} + \beta_1\,u + u^3 = P_2\,\cos\,\theta$$

<div align="right">(5.6)</div>

5.1.2. Harmonic solution of equation (5.6). - Seeking harmonic solutions for u, equation (5.6) leads to a simplified cubic equation,

$$(\beta_1 - 1)\,u + \frac{3}{4}\,u^3 = P_2$$

<div align="right">(5.7)</div>

from which u, and hence a, can be obtained.

<div align="center">5.2. Theoretical and Experimental Results</div>

Theoretical results for two configurations of the electrostatic wall are presented in figures 5 through 8. The membrane material used (commercially named Mylar) has the following properties:

$$E = 3.5 \times 10^8 \ kgf/m^2$$

$$\rho = 138\ \frac{kgf\ sec^2}{m^4}$$

$$\nu = 0.3$$

<div align="right">(5.8)</div>

The air gap between the membranes in two different configurations were H = 0,305 mm and H = 0,127 mm. Since the electrostatic forces are inversely proportional to gap height H, the smaller gap provides a larger force on the structure for a given voltage. However, the breakdown potential for the system is smaller when the gap is smaller. Hence the electrostatic forces available in both these configurations at the optimal voltage are of the same order. However the smaller air gap has the advantage that one can work with lower voltage levels.

In figures 5 and 6 the theoretical values are compared to the bench test results. It is surprising to observe such an excellent agreement between the test values and theoretical prediction. The experimental measurements of dynamic surface motion were obtained using an optical setup. Reference 10 describes in detail the measurement technique. The a.c. voltage applied to the electrodes was at 300 Hz for these experiments.

Figures 7 and 8 show the frequency response of the structure at various excitation levels. The nature of the backbone curve is indicated by dotted lines in these figures. At low excitation levels where w/h << 1, there is a steep increase in amplitude levels at resonance. At higher levels of excitation resonance has little effect on amplitude level. In the theoretical analysis structural damping was taken to be negligible. Since damping primarily affects the near resonance amplitude levels, it is not necessary to include structural damping in the response studies for the present case as can be seen from the nature of the response curves. The reason for this is very clear; viz, the test structures have resonance frequencies well above the excitation frequency for load values of interest (large amplitude case). Furthermore at these load values the nonlinear stiffnesses themselves act as a damper or delimiter on the amplitude levels. When the structural nonlinearity is of the soft spring type it might well be important to include the damping in the analysis since natural frequencies for this case are being constantly shifted downward from the low excitation case (w/h << 1) with larger excitation levels.

5.3. Examination of the Perturbation Field
Due to Primary Motion

When the membrane is set into motion by the action of an electrostatic force field, the electrical field configuration changes and consequently the excitation field itself must be reexamined.

To analyze the effect of the surface motion on the electric field configuration an orthogonal curvilinear coordinate system can be used. Since, as far as the electric field is concerned, the structural motions have a stationary behavior, a quasi-rigid coordinate mapping is required. Curvilinear coordinates such as the one to be described have been used by Benjamin (ref. 7) and Chang (ref. 8) for flow problems. The first order curvilinear orthogonal map is shown in figure 9. The amplitude of the wavy surface is taken to be (0.1 H); $Y_1 = 0.0$ curve in the figure represents the approximation to the actual surface. Since $\frac{\ell}{b} \ll 1$, the variation in the chordwise directions have been neglected just as in section 4. The mappings for this configuration are

$$\overline{x_1} = \overline{x} - a\, e^{-2\pi\overline{z}} \cos 2\pi\overline{x} \sin \Omega t$$

$$y_1 = \overline{z} - a\, e^{-2\pi\overline{z}} \sin 2\pi\overline{x} \sin \Omega t \tag{5.9}$$

$\overline{x} - \overline{y}$ coordinates can be written as

$$\overline{x} = \overline{x_1} + a\, e^{-2\pi\overline{y}_1} \cos 2\pi\overline{x_1} \sin \Omega t$$

$$\overline{z} = \overline{y_1} + a\, e^{-2\pi\overline{y}_1} \sin 2\pi\overline{x_1} \sin \Omega t \tag{5.10}$$

The solution of equation (4.1) with the boundary conditions should be attempted. We write the governing equation and the boundary conditions in the mapped system as

$$\frac{\partial^2 v}{\partial x_1^2} + \frac{\partial^2 v}{\partial y_1^2} = 0 \tag{5.11}$$

$$y_1 = 0 \qquad V = 0$$

$$y_1 = (H/\ell) \qquad V = V_0 + V_1' \sin \Omega t \sin(2\pi x_1)$$

$$x_1 = 0,\ 1 \qquad V = V_0 y_1 \tag{5.12}$$

The solution of the above problem yields

$$V_z = \frac{v_0}{H} + \left. \frac{\frac{2\pi}{\ell} V_1'}{\sinh \frac{2\pi H}{\ell}} \right\} \sin 2\pi \bar{x} \sin \Omega t$$

$$+ 2\pi a (\cos 2\pi \bar{x} \; e^{-2\pi H/\ell} - \cos 4\pi \bar{x}) \sin \Omega \tau \bigg\} \tag{5.13}$$

and

$$V_x = 0 \, .$$

The correction to the electric field distribution is therefore of the order of (w/ℓ) times its original value. For the electrostatic walls we are testing the magnitude of this correction is less than five percent when the amplitude of the surface motion is 0.025 mm at a spacing of the bay of 1.814 mm. In all the tests that we carried out the perturbation field was negligible since the excitation field could barely drive the system to these values of amplitude. An error of 15 percent in the evaluation of the electric field would usually generate an error of 10 percent in the amplitude prediction, which must be borne in mind when accuracies of that order are required.

When the deflections of the surface are quite large the perturbed field can be evaluated using a more refined (second order) coordinate system such as used by Chang (ref. 8). We show the mapped system in figure 10 and give the transformations below as

$$\overline{x_1} = \bar{x} - a \; e^{-2\pi \bar{z}} \cos 2\pi \bar{x} \sin \Omega t - \pi a^2 \; e^{-4\pi \bar{z}} \sin 4\pi \bar{x} \sin \Omega t$$

$$\overline{y_1} = \bar{z} - a \; e^{-2\pi \bar{z}} \sin 2\pi \bar{x} \sin \Omega t + \pi a^2 \left(e^{-4\pi \bar{z}} \cos 4\pi \bar{x} - 1 \right) \tag{5.14}$$

$$x = \overline{x_1} + a \; e^{-2\pi \overline{y}1} \cos 2\pi \overline{x_1} - \pi a^2 \; e^{-4\pi \overline{y}1} \sin 4\pi \overline{x_1}$$

$$z = \overline{y_1} + a \; e^{-2\pi \overline{y}1} \sin 2\pi \overline{x_1} + \pi a^2 \left(e^{-4\pi \overline{y}1} \cos 4\pi \overline{x_1} + 1 \right) \tag{5.15}$$

5.4. Inclusion of Aerodynamic Forces for
the Electrostatic Wall

The electrostatic walls were purposefully designed as small wavelength configurations. Hence, static divergence will not be achieved in any of the electrostatic walls under operating condition (15 m/s - 50 m/s) in the 7 in. × 11 in. tunnel. In reference 1, an inviscid analysis has been carried out for the evaluation of the aerodynamically induced pressure p^{aero} [eq. (39), p. 16 of ref. 1] due to structural motion.

We give this expression as

$$p^{aero} = 2\pi\rho <air> a_{11} \frac{U_\infty^2}{\sqrt{1 - M_\infty^2}} \sin 2\pi\bar{x} \sin \pi\bar{y} \sin \omega\tau. \qquad (5.16)$$

Figure 11 shows the effect of including aerodynamic loads in the analysis for the case of flow over the membrane. Our contention is fairly clear; there is no need for any sophisticated analysis of aerodynamic effects for these configurations since even the inclusion of the inviscid values which overestimate these magnitudes increases the levels of amplitude very slightly and that increase is only over a very narrow window. The a.c. voltage applied to the electrodes in this example is at 300 Hz. If the a.c. voltage was applied at very much higher frequencies the effect of the aerodynamic load on the motion will be enhanced since the effective nonlinear stiffness would be considerably lowered.

We again point out that the analysis which took into consideration the aerodynamic load was carried out under the prior known fact that the wavelength of the structures was much too short to cause static divergence; hence the flow-structure interaction problem is not of an eigenvalue type but merely a forced response problem.

6. CONCLUDING REMARKS

A unified theory for an electrostatically driven active wall system has been presented. The electrostatic wall system is capable of producing deflections of many orders of thicknesses. Consequently a large intermediate response theory has been used for analysis. The theoretical analyses are compared with bench test

results which show excellent agreements between the two. The case of an elec-
trostatic wall vibrating in the windtunnel is considered, and the theoretical
predictions under simulated flow conditions indicate that the aerodynamic
effects are negligible. The perturbation effects to the electric field due to
the structural motions are also considered and shown to be negligible for the
test experiments.

REFERENCES

1. Balasubramanian, R: Analytical and Numerical Investigation of Structural Response of Compliant Wall Materials. Final Report (Supplement No. 1) prepared for NASA, Langley Research Center, Hampton, Virginia 23665 under NSG 1236, Old Dominion University Research Foundation, Norfolk, Virginia, April 1977.

2. Kendall, J.M.: The Turbulent Boundary Layer over a Wall with Progressive Surface Waves. J. Fluid Mech., vol. 41, no. 2, pp. 259-281, 1970.

3. Mattout, R.B. Cottenceau: Etude Experimentale D'une Paroi Souple Activee En Tunnel Hydrodynamique Mesures Globales. Tn. no. 71-C1-09, Societé Bertin & Cie, 1971.

4. Merkulov, V.I.; Yu, I. Savchenko: Experimental Investigation of Fluid Flow Along a Travelling Wave. Hydrodynamic Problems of Bionics, Bionica, Keiv, vol. 4, pp. 3-120, 1970.

5. Bushnell, D.M.; Hefner, J.N.; and Ash, R.L.: Effect of Compliant Wall Motion on Turbulent Boundary Layers, Phys. Fluids, vol. 20, no. 10, Part II, pp. 531-548, Oct 1977.

6. Weinstein, L.M.; and Balasubramanian, R.: An Electrostatically Driven Surface for Flexible Wall Drag Reduction Studies. Second International Conference on Drag Reduction, BHRA Fluid Engineering, Cranfield, Bedford, U.K., pp. E5-57-E576, Sep 1977.

7. Benjamin, T.B.: Shearing Flow over a Wavy Boundary. J. Fluid Mech., vol. 6, no. 2, pp. 161-205, 1959.

8. Chang, L.: Theoretical Investigation of Turbulent Boundary Layer over a Wavy Surface. Ph.D. Dissertation, California Institute of Technology, Pasadena, California, 1975.

Table 1. Stiffness coefficients.

$$G_{11}^1 \equiv \left\{ \pi^4 \left[\left(12 - 4\nu^2\right) + \frac{7}{2}\nu\beta^2 + \frac{\beta^4}{4}\left(5 - \nu^2\right) \right] \right.$$

$$+ \frac{\pi^4\beta}{8(\nu - 1)}(\beta^2 + 4)\left[\beta^5\left(1 - \nu\right) + \beta^4\left(\frac{\nu - 1}{\pi}\right) + \beta^3\left(4\nu^2 + 12 - 16\nu\right) \right.$$

$$\left. \left. + \beta^2\left(\frac{4\nu^2 - 4\nu - 8}{\pi}\right) + \beta\left(16 - 16\nu - 16\nu^2\right) - \frac{32}{\pi}\nu \right] \right\} \frac{1}{4(1 - \nu^2)}$$

$$G_{12}^1 = \left\{ \pi^4\left[\left(8 - 16\nu^2\right) - 12\,\nu\beta^2 \right] + \frac{\pi^4\beta}{16(1 + \beta^2)^2(\nu - 1)}\left[12\left(1 - \nu\right)\beta^7 \right. \right.$$

$$\cdot \frac{\div 10\beta^6}{\pi}\left(\nu - 1\right) + \beta^5\left(-24\nu^2 + \left(21 - \frac{53}{\pi^2}\right)\nu + 56\right) + \beta^4\left(\frac{40}{\pi}\nu^2 - \frac{32}{\pi}\nu\right.$$

$$\left. - \frac{28}{\pi}\right) + \beta^3\left(44 + 92\nu - 135\nu^2\right) + \beta^2\left(\frac{32\nu^2}{\pi} - \left(\frac{112}{\pi} + 8\right)\nu\right.$$

$$\left. \left. - \frac{16}{\pi}\right) + \beta\left(16 + 96\nu - 96\nu^2\right) - 32\left(\nu^2 + \frac{2\nu}{\pi}\right) \right]$$

$$+ \frac{\pi^4\beta^2}{8(\beta^2 + 4)^2(\nu - 1)}\left[\left(9\nu\right)\beta^6 + \beta^4\left(132\nu^2 + 20\nu + 8\right) + \beta^2\left(308\nu\right. \right.$$

$$\left. \left. \left. + 296\nu^2 - 64\nu^3 - 224\right) + \left(512 - 128\nu - \left(64 + \frac{624}{\pi}\right)\nu^2 + 192\nu^3\right] \right\} \frac{1}{4(1 - \nu^2)}$$

$$G_{13}^1 = \left\{ \pi^4\left[8 + \left(20\nu\right)\beta^2 + \frac{\beta^4}{4}\left(27 - 9\nu^2\right) \right] \right\} \frac{1}{4(1 - \nu^2)}$$

$$K_{11} = \frac{\pi^4\gamma^2}{12(1 - \nu^2)}\left[16 + 8\beta^2 + \beta^4 \right]$$

$$G_{22}^1 = \left\{ \pi^4\left[\left(12 - 4\nu^2\right) + \beta^2\left(90\nu - \frac{81\nu^2}{4}\right) + \frac{243}{4}\beta^4 \right] \right.$$

$$+ \frac{\pi^4\beta}{8(\nu - 1)(9\beta^2 + 4)}\left[729\,\beta^5\left(1 - \nu\right) + \frac{243}{\pi}\beta^4\left(\nu - 1\right) + 972\beta^3\left(1 - \nu\right) \right.$$

$$\left. \left. + \frac{108}{\pi}\beta^2\left(\nu^2 - 2\right) + 144\beta\left(1 - \nu^2\right) - 96\nu \right] \right\} \frac{1}{4}\left(1 - \nu^2\right) \qquad \text{(cont'd)}$$

$$G_{21}^1 = \left\{ \pi^4 \left[8 + 20\beta^2\nu + \frac{\beta^4}{4}\left(27 - 9\nu^2\right) \right] \right\} \frac{1}{4(1 - \nu^2)}$$

$$G_{22}^1 = \left\{ \pi^4 \left[8(1 - 2\nu^2) - 12\nu\beta^2 \right] \right.$$

$$+ \frac{\pi^4\beta}{16(\beta^2 + 1)^2(\nu - 1)}\left[108\beta^7(1 - \nu) - \frac{90}{\pi}\beta^6\left(1 - \nu\right) \right.$$

$$+ \beta^5\left(504 - 346.83\nu + 168\nu^2\right) - \frac{\beta^4}{\pi}\left(252 - 32\nu\right.$$

$$\left. - 40\nu^2\right) - \beta^3\left(16 + 580\nu - 148\nu^2 + 20\nu^3\right)$$

$$- \frac{\beta^2}{\pi}\left(144 + 338.2\nu - 32\nu^2\right) + \beta\left(80 - 160\nu + 48\nu^2\right)$$

$$\left. - \left(\frac{\nu 64}{\pi} + 32\nu^2\right) \right] + \frac{\pi^4\beta^2}{8(\beta^2 + 4)^2(\nu - 1)}\left[81\beta^6\nu + \beta^4\left(72 + 180\nu + 900\nu^2\right) \right.$$

$$- \beta^2\left(992 + 128\nu - 1216\nu^2 + 1088\nu^3\right)$$

$$\left. \left. - \left(128\nu + 262.63\nu^2 - 192\nu^3\right) \right] \right\} \frac{1}{4(1 - \nu^2)}$$

$$K_{22} = \frac{\pi^4\gamma^2}{12(1 - \nu^2)}\left[4 + 9\beta^2 \right]^2 = \frac{\pi^4\gamma^2}{12(1 - \nu^2)}\left[16 + 72\beta^2 + 81\beta^4 \right]$$

CONDUCTING MEMBRANE

SEALED AIR CAVITY

EPOXY CEMENT

H_1

H

1/8 | 1/4 | 1/4 | 1/4 | 1/8

A

1

2 T

V_0

B

(a) Electrical hookup

V_A

V_B

V_0

$1 \longrightarrow$

$V_A = V_0 + V_1 \sin \omega t$

$V_B = V_0 - V_1 \sin \omega t$

$V_0 = V_1$

(b) Voltage distribution in the terminals A and B

Figure 1. The electrical arrangement of the electrostatic wall system.
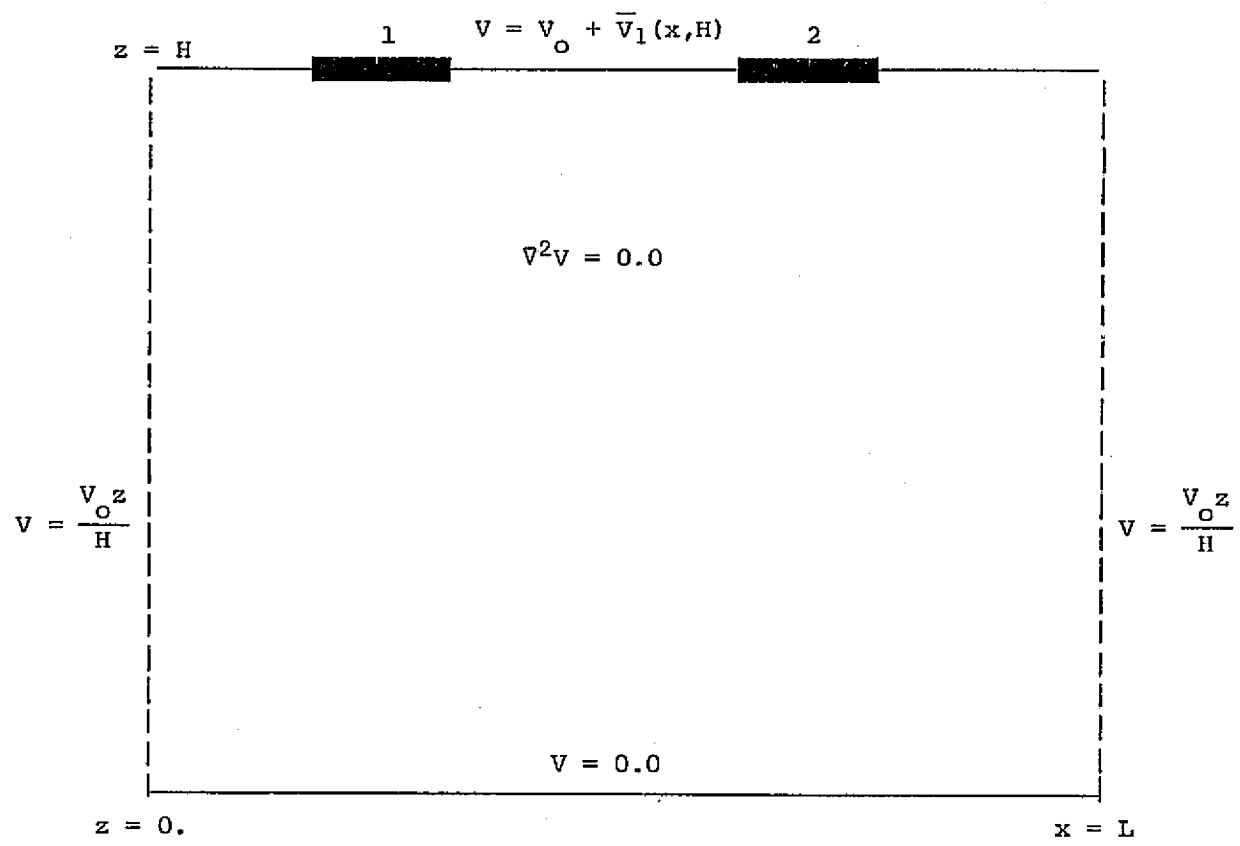
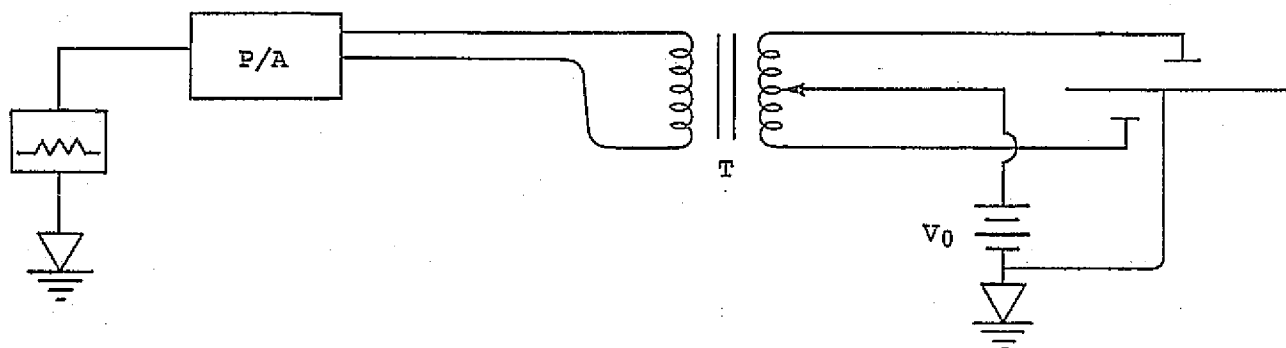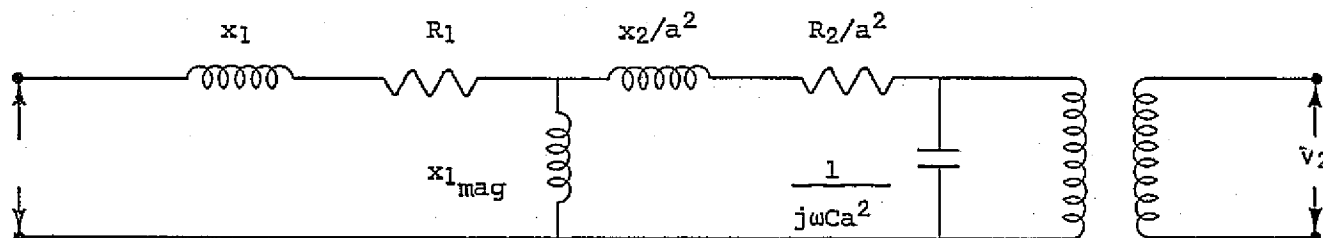Figure 2. Mathematical representation of the electrostatic field problem.
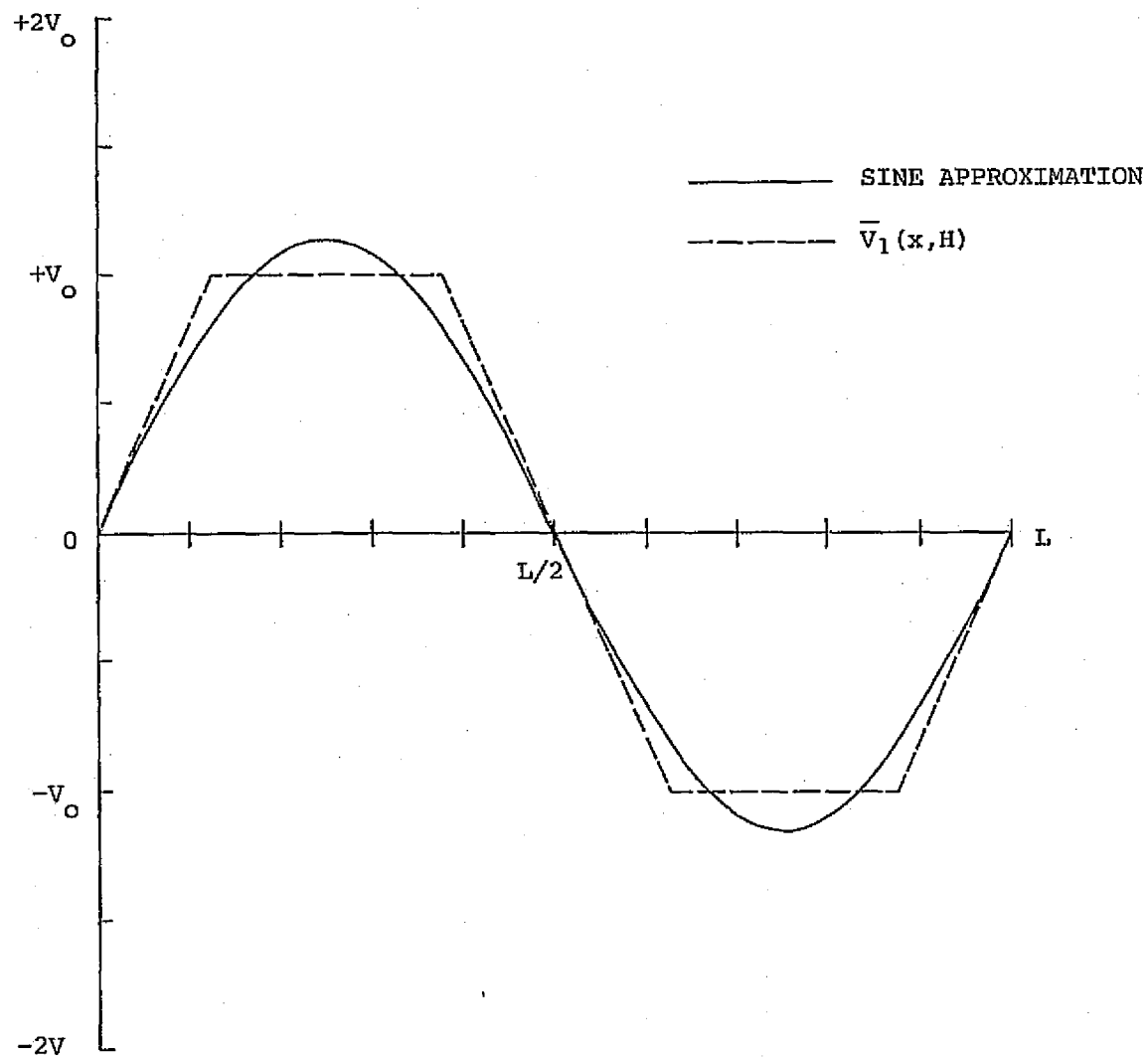
Figure 3. $\overline{V}_1(x,H)$ and its Fourier representation.

Schematic of the electrostatic wall system

Equivalent circuit

Figure 4.   Schematic of the hookup for the electrostatic wall system.
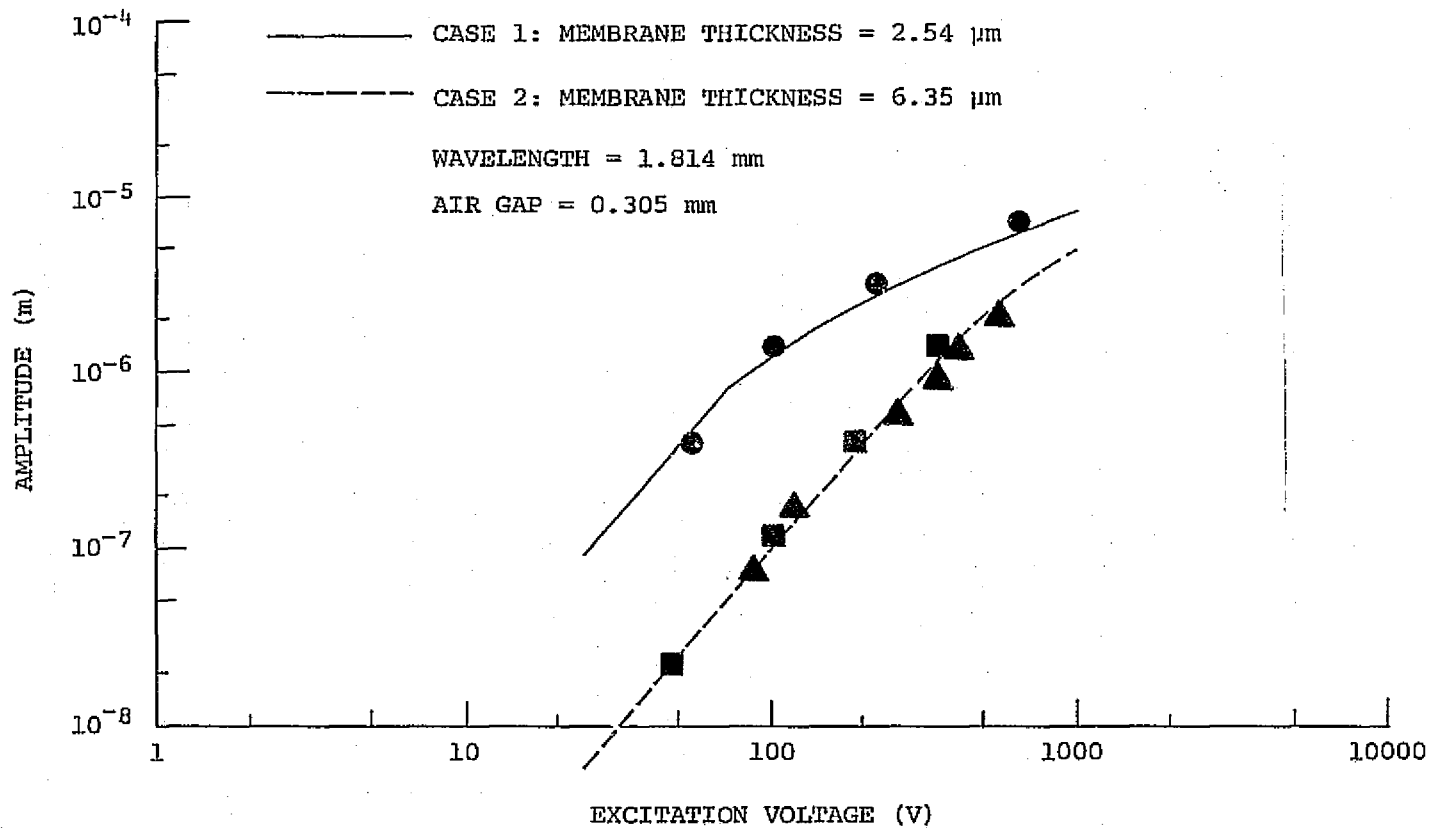
Figure 5. Theoretical response curve and test results.
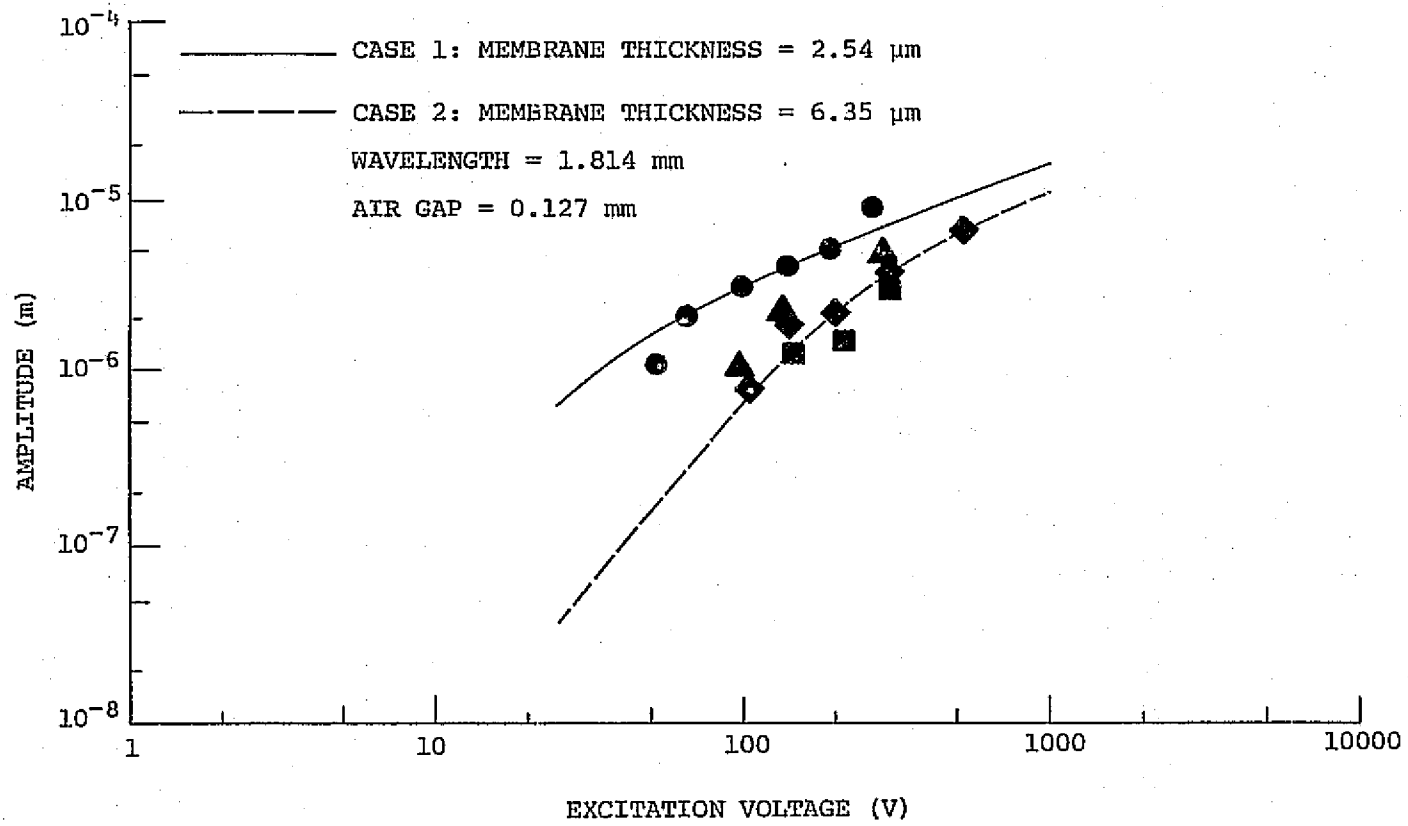
Figure 6.   Theoretical response curve and test results.

CASE 1:   MEMBRANE THICKNESS = 2.54 µm

WAVELENGTH = 1.814 mm
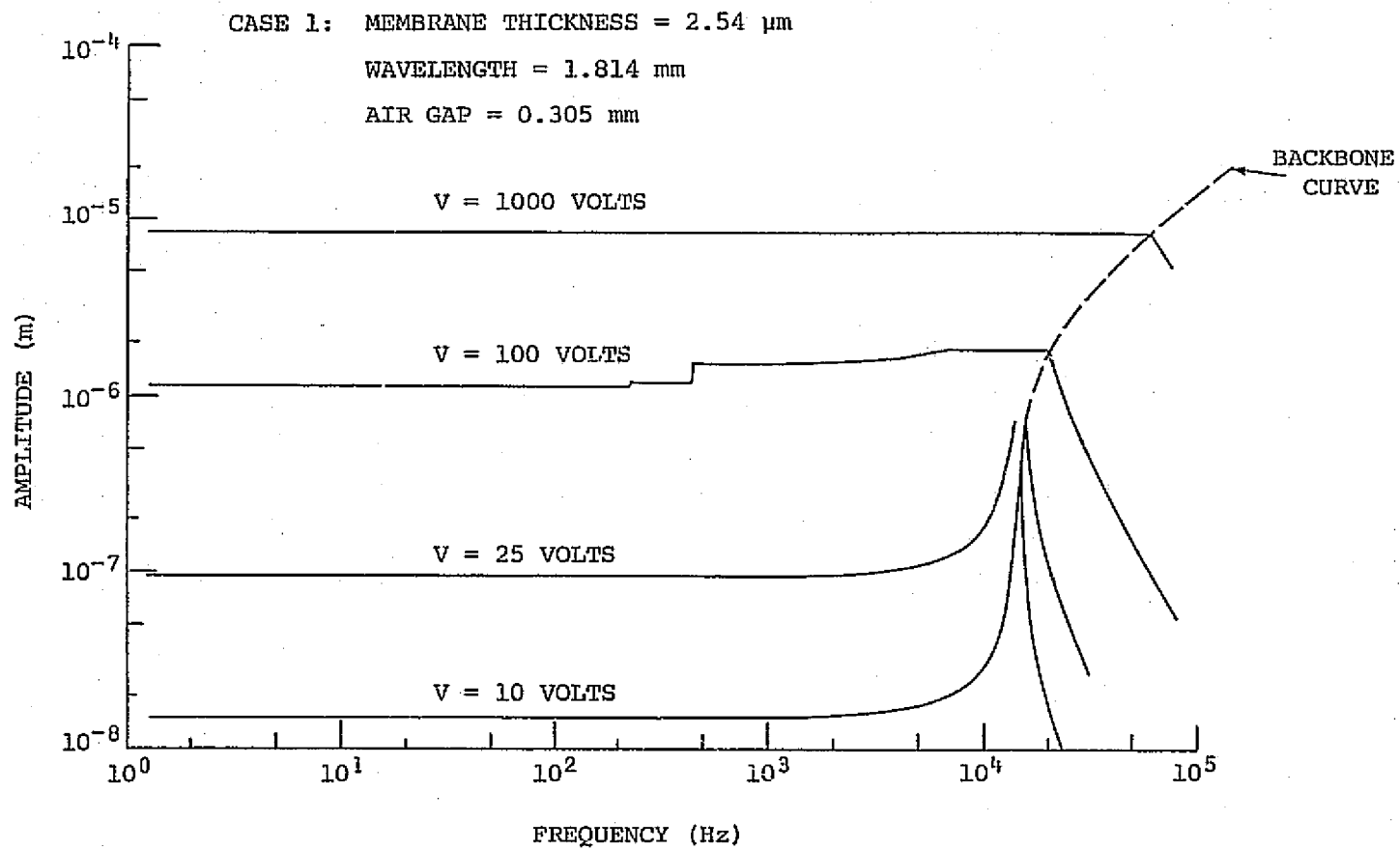
AIR GAP = 0.305 mm

Figure 7.   Frequency response curve.
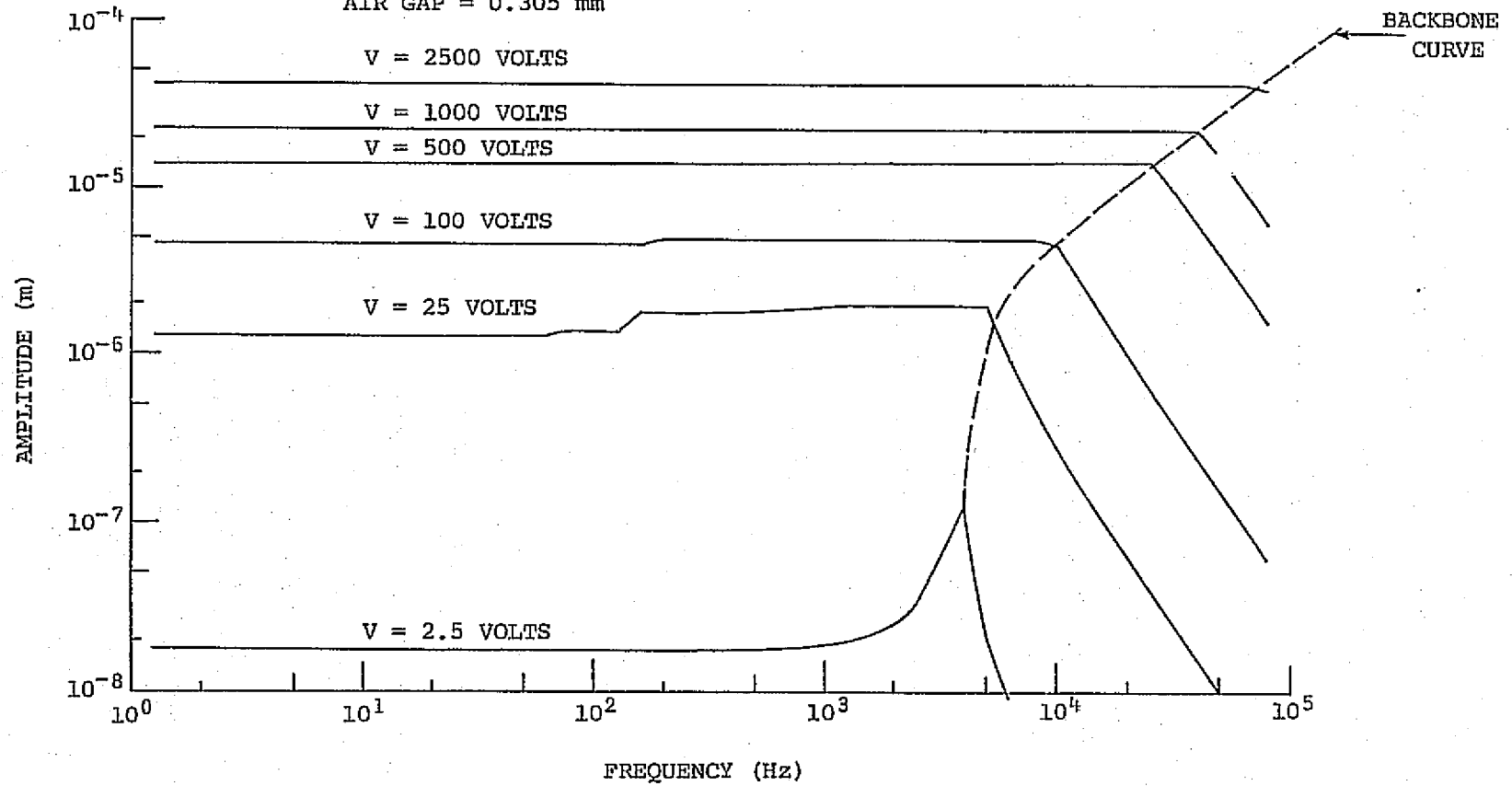
Figure 8. Frequency response curve.
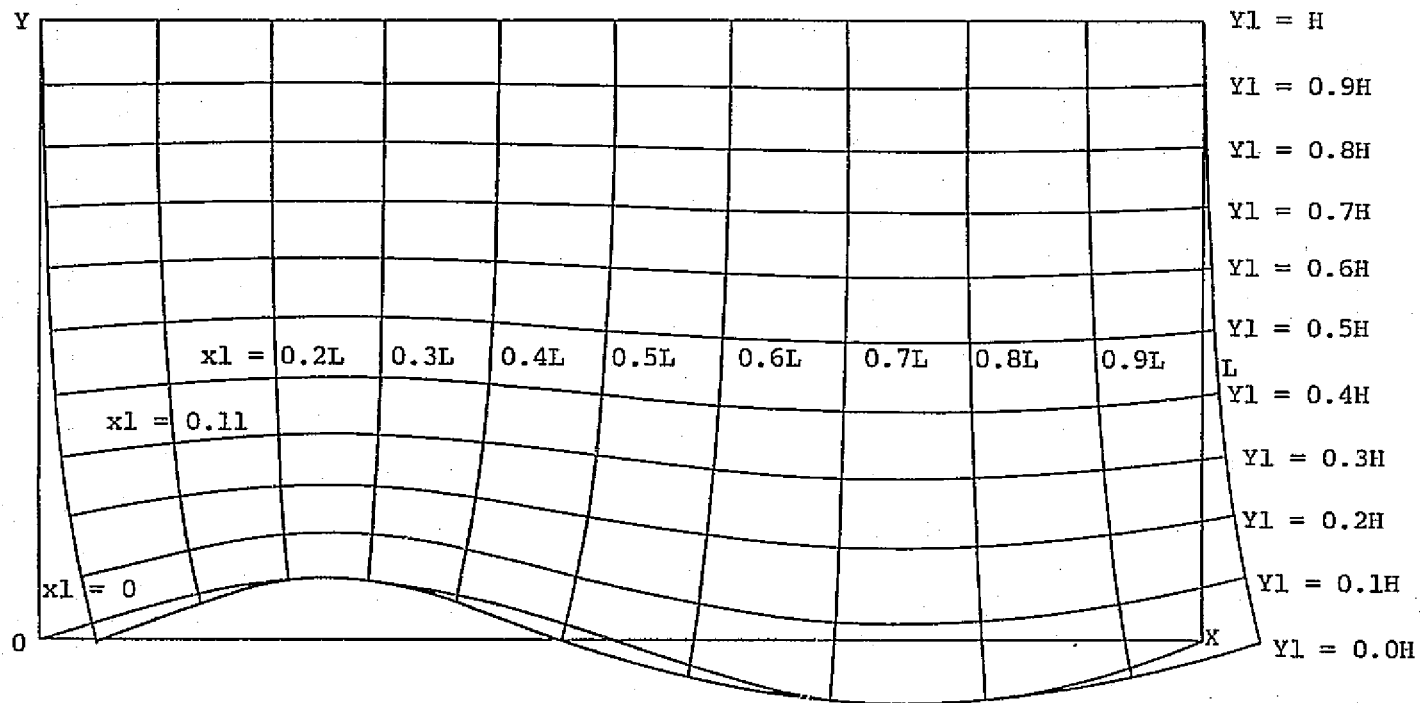
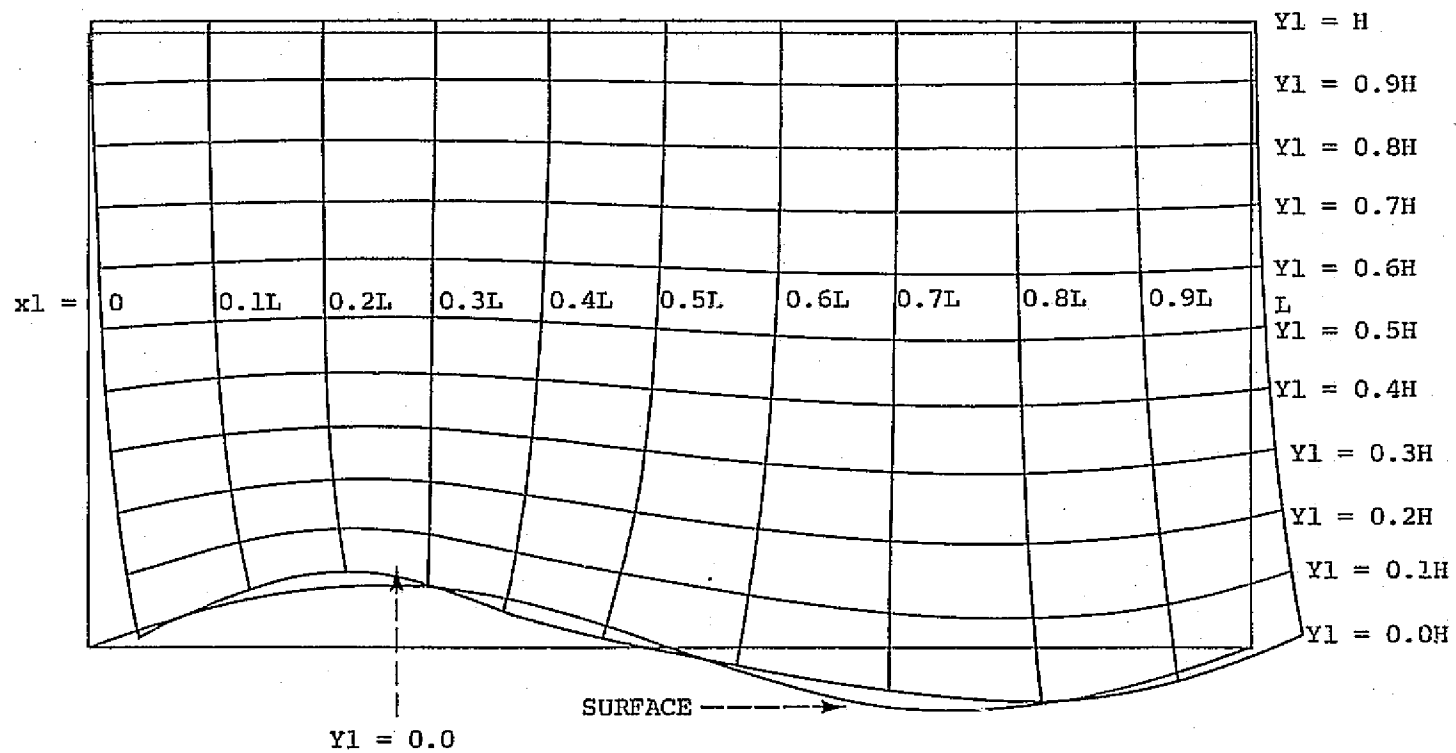Figure 9. First order orthogonal coordinate system for analysis of the perturbed field.

Figure 10. Second order orthogonal coordinate system for analysis of the perturbed field.

CASE 1: MEMBRANE THICKNESS = 2.54 μm

WAVELENGTH = 1.814 mm

AIR GAP = 0.127 mm

FREQUENCY OF EXCITATION = 300 Hz
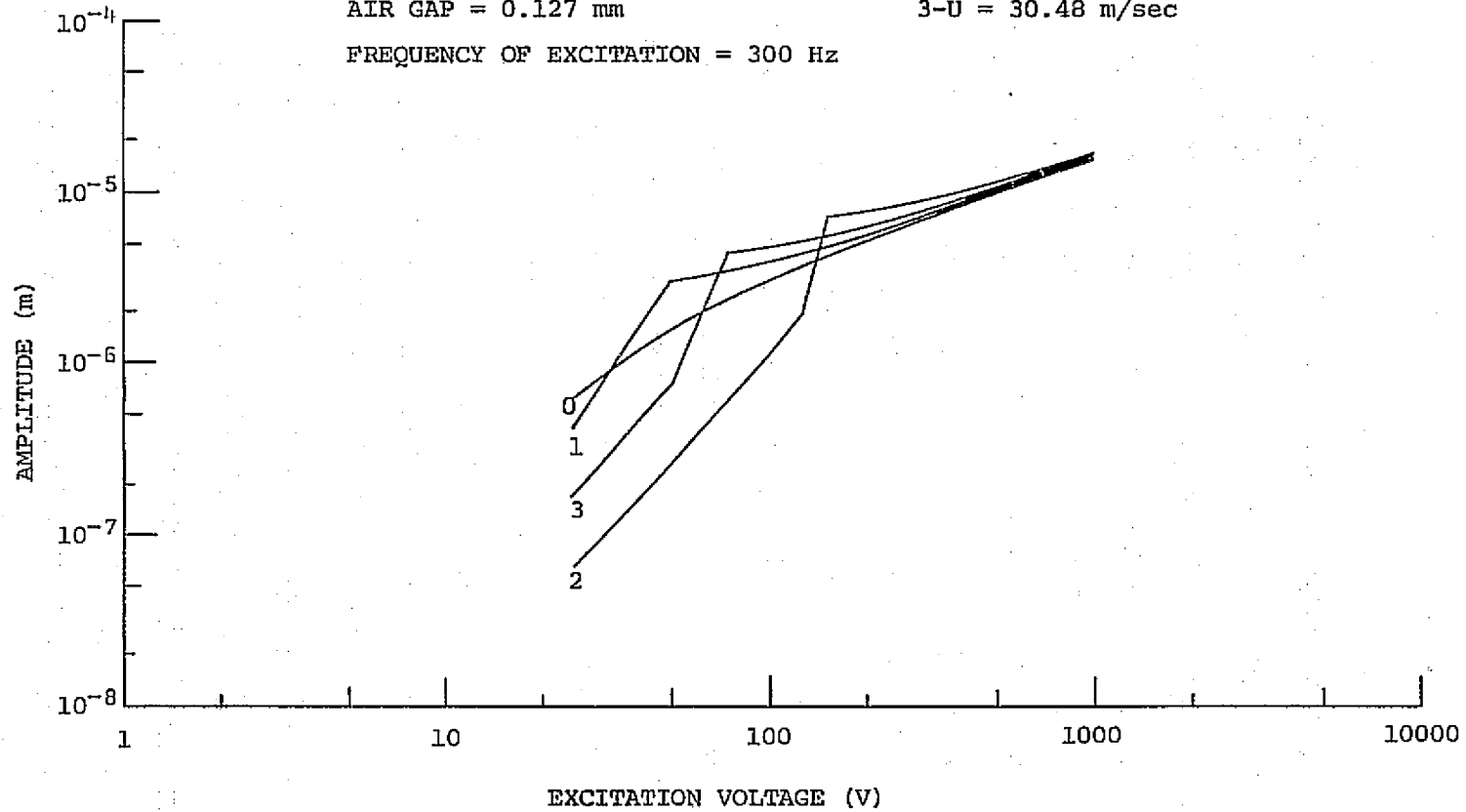
0 = NO FLOW

1-U = 22.86 m/sec

2-U = 45.72 m/sec

3-U = 30.48 m/sec

Figure 11.   Theoretical response with aeroloads.